Suppression of intestinal dysfunction in a *Drosophila* model of Parkinson's disease is neuroprotective

Giorgio Fedele [1, 2], Samantha H. Y. Loh [1, 2], Ivana Celardo [1], Nuno Santos Leal [1], Susann Lehmann [1], Ana C. Costa [1] and L. Miguel Martins[*, 1]

[1] MRC Toxicology Unit, University of Cambridge, Gleeson Building, Tennis Court Road, Cambridge CB2 1QR, UK

*Corresponding author: L. Miguel Martins, MRC Toxicology Unit, University of Cambridge, Gleeson Building, Tennis Court Road, Cambridge CB2 1QR, UK
martins.lmiguel@gmail.com

[2] These authors contributed equally to this work.

Running title: Mitochondrial toxicity in the gut drives neurodegeneration

ABSTRACT

The innate immune response mounts a defence against foreign invaders and declines with age. An inappropriate induction of this response can cause diseases. Previous studies showed that mitochondria can be repurposed to promote inflammatory signalling. Damaged mitochondria can also trigger inflammation and promote diseases. Mutations in *pink1,* a gene required for mitochondrial health, cause Parkinson's disease (PD), and *Drosophila melanogaster pink1* mutants accumulate damaged mitochondria. Here, we showed that defective mitochondria in *pink1* mutants activate *Relish* targets and demonstrated that inflammatory signalling causes age-dependent intestinal dysfunction in *pink1*-mutant flies. These effects result in the death of intestinal cells and metabolic reprogramming, and neurotoxicity. We found that *Relish* signalling is activated downstream of a pathway stimulated by cytosolic DNA. The suppression of *Relish* in the intestinal midgut of *pink1*-mutant flies restores mitochondrial function and is neuroprotective. We thus conclude that gut-brain communication modulates neurotoxicity in a fly model of PD through a mechanism involving mitochondrial dysfunction.

Keywords: *Drosophila*; mitochondria; Parkinson's disease; *pink1*, *Relish*, innate immunity, intestine, brain, gut-brain communication.

Abbreviations: PD, Parkinson's Disease; PINK1, PTEN-induced kinase 1; mtDNA, mitochondria DNA; QC, quality control; Imd, immune deficiency; TAGs; triglycerides; CNS, central nervous system; AMPs, antimicrobial peptides; ISCs, intestinal stem cells; IPCs, insulin-producing cells; DAs, dopaminergic neurons

INTRODUCTION

Animals use the innate immune system as a defence against foreign invaders, which allows a rapid reaction to invading pathogens, such as microbes. Microbes often release foreign nucleic acids into the cytosol of infected cells, which can trigger innate immunity.

Mitochondria are energy-generating organelles that evolved from endosymbionts related to bacteria. Mitochondria retain some of their genetic material in the form of DNA (mtDNA). mtDNA can trigger inflammatory responses similarly to bacterial DNA, and these responses are associated with the absence of methylated CpG sequences in both bacterial DNA and mtDNA [1].

Cells safeguard the health of their mitochondria by operating several quality control (QC) mechanisms that ensure the disposal of faulty mitochondria. The organellar QC of organelles involves the degradation of defective mitochondria via mitophagy, which is a form of autophagy (reviewed in [2]). Mutations in the gene encoding the mitochondrial kinase PINK1 lead to the accumulation of defective mitochondria and cause a form of familial Parkinson's disease (PD), an age-related neurodegenerative disease (reviewed in [2]). PINK1 functions in a molecular pathway that ensures the degradation of faulty mitochondria via mitophagy. In mice, the blockage of mitophagy induces the escape of mtDNA into the cytosol, where it activates innate immunity [3].

Constitutive activation of innate immunity in the fruit fly (*Drosophila melanogaster*), decreases lifespan and increases neurodegeneration [4]. The innate immune system in *Drosophila* consists of two branches (reviewed in [5]): the Toll signalling pathway and the immune deficiency (Imd) pathway. The Imd pathway activates the Rel/NF-κB transcription factor Relish, which controls the expression of several antimicrobial peptides and is indispensable for normal immunity in flies. Relish rewires the metabolism by attenuating FOXO-mediated lipolysis [6] and can also activate programmed cell death [7].

The main immune organs in *Drosophila* are the fat body, which is considered to be equivalent to both vertebrate adipocytes and liver, and the intestine. The intestine, in particular, plays a key role in activating the Imd pathway (reviewed in [8]).

Mounting an immune response is energetically costly and requires trade-offs with other important biological functions (reviewed in [9]), and in flies, this trade-off is

important during starvation. In such settings, *Relish* mutants exhibit increased survival when deprived of food [10]. The activation of Relish in response to cytosolic DNA can be mediated by interactions with *Drosophila* Eya, which is a molecule that maintains Relish in the cytoplasm [11].

Here, we found that in *pink1*-mutant flies, in which mitophagy is blocked, Relish was activated with neurotoxic consequences. The accumulation of defective mitochondria in these mutants lead to increased *Relish* signalling, caused intestinal dysfunction, and resulted in cell death in the midgut. Enhanced *Relish* signalling also resulted in metabolic alterations in *pink1*-mutant flies. These alterations are characterised by the accumulation of triglycerides (TAGs) due to the Relish-dependent regulation of lipid catabolism [6] and the failure of beta oxidation [12]. The genetic suppression of Relish or Eya, a Relish-binding protein involved in the sensing of cytosolic DNA, suppressed neurodegeneration in *pink1*-mutant flies. To understand the links between intestinal dysfunction and neurodegeneration, we subsequently investigated whether intestinal dysfunction could prime neurodegeneration and found that the prevention of intestinal dysfunction through either the suppression of Relish expression or the blockage of cell death in the midgut of *pink1*-mutant flies is sufficient to suppress the central nervous system (CNS) phenotypes of these flies. We conclude that the CNS defects in *pink1*-mutant flies are modulated by a non-cell autonomous signalling pathway induced by mitochondrial toxicity acting between the intestine and the brain.

RESULTS

Identification of a *Relish* signature in *pink1* mutants

We previously showed that mitochondrial defects in *pink1*-mutant flies lead to the upregulation of both nucleotide metabolism and immune response genes[12]. Here, we first explored the mechanism underlying the activation of the innate immune response pathways associated with mitochondrial dysfunction in *pink1*-mutant flies. We analysed innate immunity-related transcripts and proteins in *pink1*-mutant flies through an *in silico* approach (Figure 1A) and detected 45 upregulated transcripts that matched a curated list of innate immunity-related genes in flies (Figure 1B and Supplementary Table 1). Because *pink1*-mutant flies exhibit a global shutdown of protein synthesis [13], we also measured the levels of individual proteins in adult flies through quantitative proteomics. We detected the upregulation of nine proteins belonging to the innate immunity pathways in *pink1*-mutant flies (Figure 1B and Supplementary Tables 2 and 3). The transcriptional control of the innate immune response in *Drosophila* is mediated by signalling cascades that regulate the NF-κB - like transcription factors Dif, Dorsal and Relish (Rel) (reviewed in [14]). To identify the upstream regulators of the innate immunity signature present in *pink1*-mutant flies, we used iRegulon, a tool used for the reverse-engineering of transcriptional networks [15]. The analysis of 45 innate immunity transcripts with iRegulon matched the majority of these (27) to Rel as the top upstream regulator of the innate immunity signature in *pink1*-mutant flies (Figure 1B and C, and Supplementary Table 4).

A *Relish* mutation suppresses neuronal defects in *pink1*-mutants

In flies, mutations in *pink1* affect neuronal function, which leads to disruption of circadian rhythms in young adults [16] by preventing the secretion of neuropeptides [17] and the selective loss of dopaminergic neurons in the protocerebral posterior lateral 1 (PPL1) cluster in aged flies [18]. We subsequently tested whether mutation of the *Relish* gene in Rel^{E20}/+ flies [19] affected the neuronal phenotype of *pink1*-mutant flies. Specifically, we monitored the locomotor activity in a light-dark cycle (LD) for 7 days and confirmed that *pink1*-mutant flies show aberrant activity patterns (Figure 2A). As previously reported [20], *pink1*-mutant flies exhibited a significantly longer rest (or inactivity) duration, which was correlated with lower activity levels. Interestingly, the comparison of *pink1*-mutant flies with *pink1, RelE20/+* double-mutant flies revealed that the *Relish* mutation led to a significant rescue of the sleep-wake patterns

observed in *pink1*-mutant flies toward those of control flies (Figure 2A, red and blue). Additionally, the presence of a *Relish* mutation in the *pink1*-mutant flies was sufficient to rescue the loss of DA neurons (Figure 2B and 2C).

The activity of Relish during infection is negatively regulated by calcineurins and protein phosphatases. Calcineurins can be targeted by immunosuppressants, such as tacrolimus, which is used in human organ transplantation to lower the risk of rejection. Calcineurins are present in *Drosophila* [21], and we thus tested whether pharmacological intervention with tacrolimus could suppress both locomotor activity deficits and dopaminergic neurodegeneration in *pink1*-mutant flies. The exposure of these mutants to a diet supplemented with tacrolimus significantly improved sleep impairment (Figure 2D) and prevented the selective loss of dopaminergic neurons in the PPL1 cluster (Figure 2E). Previously it has been shown that feeding *pink1*-mutant flies with rapamycin, an inhibitor of the target of rapamycin (TOR) pathway, reduces the phosphorylation of 4E-BP1 and is neuroprotective [22]. As tacrolimus is a rapamycin derivative (rapalog), we next measured the degree of 4E-BP1 phosphorylation in *pink1* mutant flies kept on a diet supplemented with tacrolimus. We found that while *pink1* mutant flies showed a decrease in non-phosphorylated 4E-BP1 as previously shown [22], these were not altered in tacrolimus fed flies when compared to flies kept on a normal diet (Figure 2F). Collectively, these findings show that suppressing innate immunity pathways by manipulating *Relish* signalling is neuroprotective in a model of *pink1* mutation-induced mitochondrial dysfunction.

Intestinal dysfunction in *pink1*-mutant flies

Relish can induce immune responses to pathogens by inducing the transcription of antimicrobial peptides such as Attacin [23]. We subsequently monitored the activation of Relish by expressing a Rel/NF-κB reporter (Att-GFP) [24,25] and detected GFP fluorescence in several regions of the *pink1*-mutant flies, including their abdominal region (Figure 3A). A more detailed analysis of the gut showed an increase in GFP expression in the gut enterocytes of *pink1*-mutant flies (Figure 3B), which indicated the activation of Relish in the gut. Relish activation involves cleavage of an inhibitory domain on the full-length protein and translocation of the cleaved domain, Rel-68, to the cell nucleus (reviewed in [5]). The decrease in cytosolic Relish correlates with its nuclear translocation [26]. We next monitored the levels of cytosolic Relish and found lower levels of the full-length protein (Figure 3C) and increased levels of the

transcript (Figure 3D) in *pink1*-mutant flies. Taken together, these results suggest that mitochondrial dysfunction in *pink1*-mutant flies is associated with *Relish* activation. The increase in the expression of immunity-related transcripts is tightly linked to intestinal barrier dysfunction in *Drosophila* [27]. We subsequently performed a Smurf assay, which is a non-invasive method for determining the intestinal integrity in adult flies. The Smurf assay showed that *pink1*-mutant flies exhibit a compromised intestinal barrier that can partially be rescued by a mutation in *Relish* (Figure 3E).
In *Drosophila*, the fat body, which is a lipid storage reservoir, and the gut form the primary immune organs. To visualize the gut and fat body in *pink1*-mutant flies, we labelled these tissues with phalloidin (to mark the gut) and BODIPY, a fluorescent lipophilic dye that stains neutral lipids. A confocal microscopy analysis of *pink1*-mutant flies showed a ring of visceral fat (fat 'doughnut') surrounding the posterior end of the posterior midgut (anterior of the Malpighian tubule junction) (Figure 4A). Fat body cells migrate to sites of tissue damage, where they clear wound-related cell debris and upregulate antimicrobial peptides (AMPs) [24]. Given their role in cell repair and renewal, we subsequently assessed whether the recruitment of fat body cells to the midgut was associated with damage to the midgut. Mitochondrial dysfunction in *pink1* mutants causes apoptosis, a form of cell death that is associated with a fragmentation of the mitochondrial network (reviewed in [28]). Confocal analysis of mitochondria labelled with a fluorescent tag (mito-GFP) showed that gut enterocytes in *pink1* mutants have a decreased mitochondrial length (Figure 4B and C). Therefore, we next assessed the degree of apoptotic cell death in the midgut of *pink1*-mutant flies and found increased levels of the active *Drosophila* caspase Dcp-1, an apoptosis effector (Figures 4D and 4F), which is partially suppressed in *pink1, Rel*^{E20}/+ double mutant flies (Figure 4F). This indicated that *pink1*-mutant flies exhibit increased intestinal damage. Damage to the intestine also results in a robust proliferative response by intestinal stem cells (ISCs) (reviewed in [29]). We also monitored the levels of ISC proliferation using a GFP reporter for Escargot (Esg), which is expressed in these cells [30], and found an increase in the number of Esg-positive cells in *pink1*-mutant flies (Figures 4E and 4G). Taken together, these data show that mitochondrial dysfunction in *pink1*-mutant flies is associated with intestinal damage.

A *eya* mutation suppresses the neuronal defects in *pink1*-mutants

In *Drosophila*, lipid droplets act as mediators of host-pathogen interactions [31]; thus, their recruitment around the gut in *pink1*-mutant flies (Figure 4A) might underlie an infection. Mitochondrial stress in *pink1*-mutant flies causes disruption of the mitochondrial ultrastructure and damage to the mitochondrial membranes in various tissues, such as the indirect flight muscle. In mice, DNA released from mitochondria into the cytosol of cells following mitochondrial stress activates the innate immune response [32]. Because mitochondrial stress can trigger the release of mitochondrial DNA (mtDNA) into the cytosol, we assessed the presence of extramitochondrial DNA in intestinal enterocytes of *pink1*-mutant flies. A confocal analysis of cells labelled with mitochondria-targeted GFP (mito-GFP) and stained with anti-DNA showed increases in the extramitochondrial DNA levels in *pink1*-mutant flies (Figures 5A and 5B).

In *Drosophila*, the Eya protein acts in a cascade that senses undigested cytosolic DNA and activates the immune response. Eya binds to the inhibitor of nuclear factor kappa-B kinase subunit beta (IKKβ) [11] and full-length Relish [11,33] (Figure 5C). Because neuronal dysfunction in *pink1*-mutant flies is suppressed by a *Relish* mutation, we subsequently tested whether *eya* can act upstream of *Relish* in response to naked mtDNA. We noted that the mRNA levels of *Relish* target genes were decreased and the extramitochondrial DNA levels were unaltered in *pink1*-and-*eya* double-mutant flies (Figure 5D and 5B, respectively). The *eya* mutation also rescued the defects in activity observed in *pink1*-mutant flies (Figure 5E, red and blue) and the loss of DA neurons (Figure 5F). We conclude that the neurotoxic consequences of the activation of the immune response in *pink1*-mutant flies are linked to the presence of extramitochondrial DNA in the cytosol.

Relish signalling induces a starvation signature in *pink1*-mutants

Drosophila pink1 mutants exhibit an impaired circadian clock [16], and here, we found that these flies also present defects in their gastrointestinal tract. Takeout is a *Drosophila* clock-controlled hormone that is primarily involved in feeding behaviour [34] and is strongly expressed in the crop, which results in dilatation of the oesophagus that serves as a food reservoir (Figure 6A), the fat body and the antennae of male flies. Takeout expression is also induced upon starvation [34]. While, no differences in

the food intake between control and *pink1*-mutant flies (Figure 6B) were found, we detected a significant increase in the level of Takeout in *pink1*-mutant flies (Figure 6C and Supplementary Table 2). Furthermore, an analysis of the Takeout transcript levels showed that this circadian output hormone was upregulated in *pink1*-mutant flies and that this upregulation was partially suppressed in *pink1*, Rel^{E20}/+ double-mutant flies (Figure 6D). The *Drosophila* genome encodes eight different insulin-like peptides (DILPs), and four of these peptides (DILP1, DILP2, DILP3 and DILP5) are functionally similar to human insulin and are produced by neuronal insulin-producing cells (IPCs) in the fly brain (Blue, Figure 6A). Starvation, or low nutrient levels, decreases the release of DILPs by IPCs (reviewed in [35]). The increase in Takeout, a starvation marker, together with the report that another clock-regulated hormone, insulin-like peptide 2 (DILP2), is arrested in the cell bodies of IPCs in *pink1*-mutant flies [17] led us to investigate whether these flies suffer from disruptions in metabolic and energy homeostasis. First, we focused on insulin, which is known to regulate dietary metabolism [36]. A confocal analysis of an epitope tagged DILP2 [37] showed that *pink1*-mutant flies have higher levels of DILP2 in IPCs (Figure 6E), which confirmed previous observations [17]. We then measured the total content of DILP2 peptide through an enzyme-linked immunosorbent assay (ELISA)-based assay [37] and found that the levels of DILP2 in aged *pink1*-mutant flies were lower than those in the controls (Figure 6F). Systemic repression of insulin signalling leads to a FOXO-dependent activation of NFκB–Relish signalling, which results in the induction of triglyceride (TAG) metabolism upon starvation [6].

Fasting induces the mobilization of stored TAGs from lipid droplets that are used by other tissues and organs as a source of energy. We subsequently measured the TAGs in control and *pink1*-mutant flies and found significant accumulation of TAGs in both young and aged *pink1B9* flies (Figure 6G), and *Relish* mutation restored the TAG levels in old flies to the normal levels (Figure 6H), in accordance with previous findings [6,38]but did not restore DILP2 levels (Figure 6I). Taken together, these results link intestinal dysfunction in *pink1*-mutant flies to an imbalance in hormones related to feeding and changes in energy storage in adult flies.

Suppressing intestinal toxicity is neuroprotective

We previously showed that degeneration of the indirect flight muscles of *pink1*-mutant flies occurs in a non-cell autonomous manner through signalling between

neurons and muscle cells [12]. Recent findings in models of PD have shown that α-synuclein pathology occurs via inter-organ communication between the gastrointestinal tract and the brain in mice (reviewed in [39]). Like those of mice, the central nervous system and gut of flies are interconnected. The *Drosophila* brain is connected to the midgut by neurons that produce insulin-like peptide 7 (ILP7) (Figure 6A). The cell bodies of these neurons are in the abdominal ganglion, and these cells innervate the midgut/hindgut junction and the rectal ampulla (reviewed in [40]).

To test whether gut-brain communication could cause neurotoxicity in *pink1*-mutant flies, we first suppressed *Relish* expression in the gut by RNAi using the NP3084 gut-specific [41,42] Gal4 driver. This downregulation of *Relish* in the gut decreased the overall levels of TAGs in *pink1*-mutant flies (Figure 7A) and increased the level of fatty acid oxidation (Figure 7B). However, suppression of *Relish* in the gut failed to block the increase in cytosolic DNA in gut enterocytes (Figure 7C). Nevertheless, *Relish* downregulation improved the mitochondrial function in the brains of *pink1*-mutant flies (Figure 7D); suppressed the inactivity defects (Figure 7E) and rescued the loss of DA neurons (Figure 7F). We next used another independent Gal4 driver, NP1[42], to confirm that suppression of *Relish* in the gut blocked neurodegeneration (Figure 7F) as well as the specificity of the NP3084 driver (Figure 7G). To rule-out the possibility that *Relish* expression causes neurotoxicity through a cell-intrinsic mechanism we also suppressed its expression directly in DA neurons using the Tyrosine Hydroxylase (TH) driver. This failed to suppress the loss of DA neurons in *pink1*-mutant flies (Figure 7F). We reason that the neurotoxic consequences of the activation of the immune response in *pink1*-mutant flies are linked to a gut-brain communication mechanism.

We subsequently tested whether the blockage of cell death in the intestine of *pink1*-mutant flies was sufficient for the suppression of neurotoxicity. We targeted the expression of either Buffy, a *Drosophila* Bcl-2-like protein with anti-apoptotic activity [43], or re-expressed Pink1 in the gut of *pink1*-mutant flies using the NP3084 driver. We found that the expression of either Buffy or Pink1 decreased the number of DCP1-positive cells (Figures 8A and 8B) and prevented the loss of DA neurons in *pink1*-mutant flies (Figure 8C). Next, we tested if suppressing *pink1* expression in the gut was sufficient to cause the degeneration of neurons with healthy mitochondria. The RNAi-mediated suppression of *pink1* using the NP3084 driver decreased the levels of the *pink1* transcript in the intestine but failed to induce a loss of PPL1

neurons (Figure 8D and 8E). We thus conclude that the suppression of intestinal dysfunction in *pink1*-mutant flies is sufficient for rescuing neurotoxicity.

DISCUSSION

Mitochondria tune their performance to adjust their energy output to the requirements of individual cells. To achieve this tuning, mitochondria communicate with the cell nucleus using the retrograde response [44], which modifies the flow of information in cells by altering the transcriptional control of cellular functions. Here, we found that Relish signalling serves as a retrograde response pathway that is activated by mitochondria and has neurotoxic consequences. Relish, the *Drosophila* orthologue of NF-κB in mammals, controls the expression of several immunity genes. Recent studies in humans and mice have shown that PINK1 plays a role in restraining innate immunity and that inflammation plays a positive role in PD [45]. Here, we extend these observations and demonstrate that in flies, this inflammatory response is triggered in the intestine and communicated to the central nervous system. These conclusions build on the increasing body of evidence obtained from models of α-synuclein pathology (reviewed in [39]) that show a role for the gut-brain axis in the aetiology of PD.

We detected increased levels of enterocyte cell death in the intestines of *pink1*-mutant flies (Figure 4). In *Drosophila,* Relish drives the removal of cells that are perceived unfit via apoptotic cell death [46], and we reason that the release of DNA from defective mitochondria in *pink1*-mutant flies labels cells as unfit and prone to Relish-mediated apoptosis. It is also possible that a defective intestinal barrier in *pink1*-mutant flies allows the invasion of gut bacteria in the intestine and activates an inflammatory response.

In *Pink1*-knockout mice, mitochondrial dysfunction induces an inflammatory response via the cGAS-STING pathway that senses cytosolic DNA and acts upstream of the Relish orthologue NF-κB [45]. In *Drosophila*, dmSTING functions downstream of Relish to control viral infection [47], and a previous study showed that its loss of function does not rescue the *pink1*-mutant phenotype [48]. Our data (Figure 5) suggest that *eya* can act upstream of Relish to sense cytosolic DNA released by defective mitochondria in *pink1*-mutant flies.

Taken together, the data from both mice[45] and flies (our study), suggests that the increased activation of NF-κB might be a risk factor for the initiation or progression of PD, associated with mitochondrial dysfunction.

The overexpression of relish in glial cells but not in neurons causes neurodegeneration in the central nervous system of flies [49]. This suggests that the neurotoxicity induced by Relish is non cell autonomous. It is therefore possible that the activation of inflammatory pathways by the overexpression of constitutively active Relish in the gut of *pink1* mutant flies would exacerbate their phenotype. This would further support the concept that immune dysfunction in the gut is a risk factor for PD. Epidemiological evidence suggests that the risk of PD is increased in inflammatory bowel disease, a chronic condition that is usually diagnosed in young individuals (reviewed in [50]). Further work is required to understand how early gut inflammation contributes to the vulnerability of neurons with impaired mitochondrial function. This will improve our understanding of disease pathogenesis and has the potential to provide new therapeutic targets.

We show that a dietary supplementation with tacrolimus, an immunosuppressant is neuroprotective in *pink1*-mutant flies. Tacrolimus is a rapalog but, contrary to tacrolimus, rapamycin is described to have immunostimulatory activity (reviewed in [51]). We therefore reason that the neuroprotective roles of these two drugs might act by activating distinct signalling pathways.

The defects in insulin signalling observed in *pink1* mutants result from the abnormal trafficking of lipids between mitochondria and the endoplasmic reticulum, which in turn affects the formation of lipid vesicles and the release of neuropeptides such as DILPs [17]. These defects in lipid trafficking arise from the increased contacts between mitochondria and the endoplasmic reticulum observed in *pink1*-mutant flies [13,17]. Although partial suppression of *Relish* rescued the lipid defects in $pink1^{B9}$ flies (Figure 6H), it did not rescue the release of DILP2 (Figure 6I), confirming previous reports that insulin signalling acts upstream of Relish [25].

Low levels of insulin are often associated with nutrient deficits and starvation, as indicated by an increased expression of Takeout (Figures 6C and 6D) [34], which results in reduced inhibition of FOXO by Akt and thus promotion of a stress response [52]. However, Relish can shape metabolic adaptation by attenuating FOXO-mediated lipolysis [6], which leads to the accumulation of lipids [53]. Therefore, the sustained

activation of Relish in *pink1*-mutant flies is likely to lead to the accumulation of lipids by blocking FOXO-mediated lipolysis.

We observed an accumulation of TAGs in *pink1*-mutant flies. Mitochondrial impairment has been shown to result in TAG accumulation [54]. We previously reported that dicarboxylate fatty acids are increased in *pink1* mutants, and this increase is likely linked to defects in fatty acid beta oxidation [12]. Therefore, the accumulation of TAGs in these mutants might result from the failure of fatty acid beta oxidation due to mitochondrial impairment. This is further supported by the observation of normal feeding in *pink1*-mutants compared to control, i.e. the starvation phenotype does not seem to arise from low food intake, but rather impairment of nutrient absorption by the gastrointestinal tract.

In rodents, the gut-brain transmission of PD pathology by α-synuclein occurs via the vagus nerve in mice [39]. Both retrograde and anterograde vagal transport act to promote the bidirectional propagation of α-synuclein toxicity to the brain and other organs in rats [55].

Our results (Figures 7 and 8) show that a gut-brain pathway is involved in neurotoxicity in a *Drosophila* model of PD. However, unlike the results obtained in α-synuclein models, our model showed that this pathway does not involve the transport of a toxic protein but rather a signal induced by defective mitochondria.

In *Drosophila*, neurons with cell bodies in the posterior segments of the abdominal ganglion of the ventral nerve cord (VNC) send axons that reach the posterior portion of the midgut (reviewed in [40]), which is the region where we detected intestinal dysfunction in *pink1*-mutant flies. Because this link between the intestine and the CNS via the VNC is established by ILP7 neurons (Figure 6A), these neurons, like the vagus nerve in rodents, might mediate toxicity between the midgut and brain in *pink1*-mutant flies. It would be interesting to test whether silencing the activity of these neurons would affect CNS toxicity in *pink1*-mutant flies.

Alternatively, the communication of toxicity from the intestine to the CNS in *pink1*-mutants could involve an indirect (humoral) mechanism(s). *pink1* mutants have impaired energy metabolism. Metabolic alterations due to starvation are known to cause mRNA downregulation of the hormone Bursicon (*burs-a*) in the gut. Recent studies have shown that Bursicon is involved in a neuronal relay to both the adipose tissue [56] and the CNS [57] and can regulate sleep via an indirect modulation of the dopaminergic system[57]. Given that our data indicates that silencing *Relish* in the gut

leads to a metabolic improvement, a rescue in PPL1 loss and sleep deficits, we investigated a possible link between Relish signalling and *burs-a* expression. We measured the levels of Bursicon mRNA in *pink1*-mutant flies and found that the suppression of *Relish* increased the mRNA levels of *burs-a* in the gut of *pink1*-mutant flies (Figure 8F). It is therefore plausible that impaired Bursicon signalling acts as humoral mechanism to relay toxicity from the intestine to the CNS. Although this requires further work, we propose that the suppression of IMD pathway rescues the normal gut homeostasis, restoring Bursicon levels. The hormone in the haemolymph will then relay the nutrient information via its neuronal links both to the adipose tissue (via AKH) and potentially to the CNS where the Bursicon receptor, rickets, is expressed in a small population of neurons. Moreover, *pink1* mutants have increased sleep, which can be explained by a combination of IMD activated system [58] with reduced dopaminergic signalling (loss of PPL1) and possibly reduced Bursicon levels. This potential mechanism is being investigated by our team.

An alternative, but not mutually exclusive mechanism of humoral-induced neurotoxicity, is provided by a previous study showing that AMPs induced by Relish activation directly induce mitochondrial depolarisation, in particular AMPs targeting Gram-negative bacteria [59]. AMPs in the intestine of *pink1*-mutant flies might act as a humoral signal to induce the loss of mitochondrial membrane potential in the CNS of these flies.

Also, a third scenario, based on observations by Clark and colleagues [60], where the damage to the intestinal barrier observed in *pink1*-mutants would cause systemic inflammation due to the leakage of gut microbes into the surrounding tissues. This last scenario would be an indirect mechanism to mitochondrial impairment and lead to an alternative parallel pathway for inducing inflammation.

Our data add to an increasing body of evidence showing that signals from the gut can modulate brain activity. More specifically, our results suggest that mitochondrial toxicity in the gut can contribute to adverse effects in the brain and that therapeutic interventions aiming to decrease gut toxicity might be a viable approach for restoring brain health in diseases caused by mitochondrial compromise.

METHODS

Genetics and *Drosophila* strains

The fly stocks and crosses were maintained on standard cornmeal agar media at 25°C. The strains used were the following: *pink1*^{B9}, *white*^{1118} and *w; elav>GAL4*, which were previously described (Tufi *et al.,* 2014), *Canton-S* backcrossed to *w*^{1118} (Fedele *et al.,* 2014), *w;; Rel*^{E20} (BDSC_55714); *P{ppl-GAL4.P}2*, *yw; AttacinA::GFP* (gift from A. Franz Lab), *yw;; ILP2 HF* (gift from A. Telemans), *w; eya*^{2} (BDSC_2285), *w; UAS Relish RNAi* (VDRC_*P{KK109851}VIE-260B*), *w; +; UAS pink1 RNAi* (BDSC_31170), *w***; P{GawB}NP3084* (KSC_113094), *w; UAS-Buffy* (gift from L. Quinn), *w; UAS-Pink-HA* (gift from A. Whitworth), *THGal4* (BDSC_8848), *w; ESG>GFP; TubGAL80*^{ts} and *w[*]; P{w[+mW.hs]=GawB}Myo31DF[NP0001] (NP1>Gal4)* (gift from J. Cordero).

To distinguish *pink1*^{B9} flies from flies with X-nondisjunction, we crossed *pink1*^{B9} females to the *Canton-S* wild-type strain backcrossed to *w*^{1118}; thus, flies with nondisjunction have red eyes. This strategy was used for all crosses with mutants (*i.e., Rel*^{E20} and *eya*^{2}). For all other crosses, the flies were crossed to males carrying the FM7 balancer on the first chromosome, *i.e., pink1*^{B9}*; NP3084Gal4* x *Fm7a; UAS-RelKK*. All experiments involving adult flies were performed with males aged 3 to 5 days unless otherwise stated.

Microarray acquisition and analysis

RNA was obtained from male adult flies (six samples in total, three replicates of each genotype). The RNA quality was confirmed using an Agilent 2100 Bioanalyzer (Agilent Technologies, CA, USA). Detailed descriptions of the experimental protocols and raw data have been deposited in ArrayExpress under accession E-MTAB-6210. Differential expression was analysed using Partek Genomics Suite (Partek Inc., MO, USA) with an ANOVA model.

Proteomics analysis

Protein extracts from whole flies were prepared by grinding flies in radioimmunoprecipitation assay buffer (RIPA) (20 mM Tris pH 7.5, 150 mM NaCl, 1% (v/v) Nonidet P40, 0.5% (w/v) sodium deoxycholate, and 1 mM EDTA) supplemented with 1 µg/mL leupeptin, 1 µg/mL antipain, 1 µg/mL chymostatin, 1 µg/mL pepstatin and phosphatase inhibitor cocktail (PhosSTOP, Roche). The

suspensions were cleared by centrifugation at 21,000 g and 4°C for 10 minutes, and the protein concentrations of the supernatants were measured using the Bradford assay (Bio-Rad). The cleared lysates were stored at -80°C until proteomics analysis. TMT labelling was performed according to the manufacturer's recommended protocol (https://www.thermofisher.com/order/catalogue/product/90110). One hundred micrograms of each digested protein sample were labelled individually with each of the 10 TMT tags. After labelling, the samples were combined, cleaned on a Sep-Pak C18 cartridge, dried and dissolved in 20 mM ammonium formate (pH 10). TMT peptide fractionation was performed using an Acquity ethylene-bridged hybrid C18 UPLC column (Waters; 2.1 mm i.d. x 150 mm, particle size of 1.7 µm). Dried fractions were separated using the LC-MS/MS method as detailed below. The fractions were combined into pairs (i.e., the first fraction with the middle fraction) and analysed by LC-MS/MS using a Dionex Ultimate 3000 RSLC nanoUPLC (Thermo Fisher Scientific Inc, Waltham, MA, USA) system and a Lumos Orbitrap mass spectrometer (Thermo Fisher Scientific Inc, Waltham, MA, USA). The mass spectrometry proteomics data have been deposited to the ProteomeXchange Consortium via the PRIDE partner repository with the dataset identifier PXD030979.

Data analysis

To explore the transcriptional changes in genes involved in the *Drosophila* immune response, transcripts with fold-changes (FCs) ≥ 2 in *pink1*-mutant flies were cross-checked with a list of *Drosophila* genes potentially involved in the immune response, which was made available as a resource by the Lemaitre group (lemaitrelab.epfl.ch). The transcripts with FCs ≥ 2 in *pink1*-mutant flies annotated to this list were then analysed using the iRegulon algorithm [15] in Cytoscape (v3.5.1). A total of 45 upregulated transcripts were classed as nodes for iRegulon analysis. We used the default parameters in iRegulon that search for transcription binding motifs from 5,000 bases upstream of the full transcript. The network for nodes connected to the top enriched transcription factor (Relish) was visualised in Cytoscape (see Figure 1C). For proteomics analysis, the raw data files were processed using Proteome Discoverer v2.1 (Thermo Fisher Scientific) and Mascot (Matrix Science) v2.6. The data were aligned with the UniProt data from *Pseudomonas aeruginosa* (5584 sequences), which is the common repository of adventitious proteins (cRAP, version 1.0). All comparative analyses were performed with the R statistical language. The R package

MSnbase [62] was used for the processing of proteomics data. Briefly, this process entailed the removal of missing values (instances where a protein was identified but not quantified in all channels were rejected from further analysis), log2-transformation of the raw data, and subsequent sample normalization utilizing the 'diff.median' method in MSnbase (this translates all samples columns such that they all match the grand median). The differential abundances of the proteins were evaluated using the limma package, and the differences in protein abundances were statistically analysed using Student's t-test with their variances moderated by the empirical Bayes method in limma. The *p*-values were adjusted for multiple testing using the Benjamini Hochberg method [63].

Locomotor assays

Three- to four-day-old males were individually loaded into Drosophila Activity Monitors (DAM5) within 8 × 65-mm glass Pyrex tubes (Trikinetics, Waltham, MA, USA) containing normal fly food. The flies were maintained at 25°C under a 12-hour light:12-hour dark (LD) cycle for at least 8 days. Sleep and activity data were analysed using the Sleep and Circadian Analysis MATLAB Program (SCAMP) developed by the Griffith lab [64]. The analyses were performed for 7 days starting at the first ZT0 to allow acclimation. At least 16 flies of each genotype were used. Flies with Rhythmic Index Score below 1 were removed from the analyses.

Assay of the integrity of the intestinal barrier

We measured the integrity/functionality of the intestinal barrier by detecting the presence of a nonabsorbable blue food dye outside the digestive tract after feeding [65]. The flies were transferred to food containing 2.5% w/v Erioglaucine (FD&C Blue dye1-SIGMA) overnight [66]. Afterward, the flies were allowed to eat normal food for an additional 24 hours and then retransferred to dye-containing food for an additional 24 hours. The flies were scored after being fed normal food for 48 hours. Notably, in the analysis of Smurf flies fed normal food for 48 hours, a stained abdomen served as an indication of GI dysfunction, and we did not score different degrees of "smurfness". A pairwise test followed by a stack of *p*-values with an FDR of 10% was used to detect the significance of the differences among genotypes.

Drug treatments

Tacrolimus (FK-506 monohydrate, Sigma, F4679) was incorporated into the fly food to a final concentration of 5 mM. Flies treated with tacrolimus were transferred to drug-containing food up to 24 hours after hatching.

Protein extraction and western blotting

Flies gut samples: ten to fifteen guts were dissected in PBS and maintained on ice until ready to be processed. Protein extraction was performed using NE-PER™ Nuclear and Cytoplasmic Extraction Reagents (Thermo Scientific, 78833) following the manufacturer's instructions. The samples were separated using BioRad Precast gels and wet-blotted onto nitrocellulose membrane. The membranes were blocked in TBS (0.15 M NaCl and 10 mM Tris-HCl, pH 7.5) containing 10% (w/v) dried non-fat milk for 1hr at room temperature, then probed with the primary antibodies before being incubated with the appropriate HRP-conjugated secondary antibody. Antibody complexes were visualised by Pierce enhanced chemiluminescence (ECL).
Whole flies samples: Protein extracts from whole flies were prepared by grinding flies in RIPA buffer [0.15 M NaCl, 1% (v/v) Triton X-100, 0.5% (m/v) sodium deoxycholate, 0.1% (v/v) SDS and 50 mM of Tris (pH = 7.5)] supplemented with 1x phosphatase and protease inhibitor. Tissue and cell debris were spun down at 14.000*g* for 10 min and supernatant collected. 30µg of protein were loaded in Novex Tris-Glycine precast gels (ThermoFisher Scientific) and wet-blotted onto nitrocellulose membrane. Membranes were blocked in TBS (0.15 M NaCl and 10 mM Tris-HCl, pH 7.5) containing 5% (w/v) dried non-fat milk for 1hr at room temperature, then probed with the primary antibodies before being incubated with the appropriate IRDye-conjugated secondary antibody. Antibody complexes were visualised using Odyssey (LI-COR, Cambridge, UK), and quantifications were performed using Image Studio Lite version 5.2.5 (LI-COR, Cambridge, UK), with normalisation to the respective loading control (actin).

Antibodies and dyes

The primary antibodies and dyes employed in this study were anti-α-tubulin (CST, 2125, 1:1000), anti-cleaved *Drosophila* Dcp-1 (CST, 9678, 1:100), anti-HA (Roche Applied, 11583816001, 1:1000), anti-HA-HRP (Roche Applied, 12013819001, 1:350), anti-FLAG M2 (Sigma, F1804, 1:500 for ICC, 2.5 µg/ml for ELISA), anti-TH

(Immunostar, 22941, 1:50), anti-GFP (Abcam, ab13970, 1:1000), anti-Relish (RayBiotech, RB-14-0004-20, 1:500), anti-ds DNA (Abcam, ab27156, 1:100), anti-Non-phospho-4E-BP1 (Cell Signalling, 4923, 1:1000), anti-actin (Sigma, A1978, 1:1000), rhodamine phalloidin (Thermo Scientific, R415, 1:1000) and BODIPY 493/503 (Thermo Scientific, D3922, 1:1000). The secondary antibodies were goat anti-chicken IgY H&L Alexa Fluor 488 (Abcam, ab 150173, 1:500), goat anti-rabbit IgY H&L Alexa Fluor 488 (Abcam, ab 150077, 1:500), goat anti-mouse IgY H&L Alexa Fluor 488 (Abcam, ab 150117,1:500), goat anti-mouse IgG H&L Alexa Fluor 555 (Abcam, ab150118, 1:500), donkey anti-mouse (LI-COR, 926-32212, 1:20,000) and donkey anti-rabbit (LICOR, 926-32213, 1:20,000).

RNA extraction and quantitative real-time RT-PCR

Total RNA was extracted from 10-15 freshly dissected guts using TRIzol (Ambion) and quantified by spectrophotometric analysis (Nanodrop, Thermo Scientific). Quantitative real-time PCR with reverse transcription (qRT–PCR) was performed with a real-time cycler (Applied Biosystems 7500 Fast Real-Time PCR Systems) using the SensiFAST SYBR Lo-ROX One-Step Kit (Bioline). Fold change was calculated using the comparative CT method. For qRT-PCR, we measured the coefficient of variation (CV) of the technical replicates and excluded from statistical analysis samples with a CV over 3%. Gene-specific primers were designed with Primer3 (Primer3 Input) and FlyPrimerBank (DRSC FlyPrimerBank (flyrnai.org)) and subsequently obtained from Sigma: *Relish* – forward, 5'-CATCAGGAGACAGAGCGTGA-3', reverse - 5'- CCGACTTGCGGTTATTGATT -3; *Attacin-A* – forward, 5'- TCGTTTGGATCTGACCAAGGGCAT-3', reverse - 5'-TTCCGCTGGAACTCGAAACCATTG -3; *Turandot A*– forward, 5'-GCACCCAGGAACTACTTGACATCT -3', reverse - 5'-GACCTCCCTGAATCGGAACTC -3; *Pink1* – forward, 5'-AAGCGAGGCTTTCCCCTAC-3', reverse - 5'-GCACTACATTGACCACCGATTT-3; *Bursicon* – forward, 5'-CATCCATGTGCTCCAGTATCC -3', reverse - 5' GGCTTCACTTTGGGAACAGAA -3. *Takeout* primer was obtained from QIAGEN (QuantiTect Primer Assays, QT0098241). *rp49* was used as a housekeeping gene: *rp49* – forward, 5'- TGTCCTTCCAGCTTCAAGATGACCATC-3', reverse - 5'-CTTGGGCTTGCGCCATTTGTG-3.

Immunofluorescence and confocal microscopy

For brain imaging, the flies were fixed overnight at 4°C in 4% PFA/1% Triton/PBS. The brains were subsequently dissected in ice-cold PBS and blocked in 10% normal goat serum PBS/0.5% Triton overnight. Primary staining was performed at 4°C for 3 days, whereas the samples were incubated with the secondary antibodies for 2 hours at room temperature.

For intestinal imaging, the guts were dissected from live flies in PBS and fixed in 4% PFA for 1 hour on ice. The staining protocol was identical to that used for the brain samples.

For DCP-1(CST, 9678, 1;100) staining, the guts were fixed in heptane-methanol fixative. The samples were mounted in Vectashield (Vector Laboratories), and fluorescence images were acquired with a Zeiss LSM880 confocal microscope. Colocalisation of anti-dsDNA (Abcam, ab27156, 1:100) and mitoGFP were analysed with the colocalisation tools in ZEN Blue version 2.6. Pearson coefficient calculates pixel-based overlap of the fluorescence channels under analysis. A Pearson correlation coefficient of 1 indicates a perfect correlation between two image channels. Images were obtained from five 10 microns region of interests (ROI) per gut and at least 9 guts were analysed per genotype.

Microscopy-based assessment of mitochondrial function and morphology

Measurements of the $\Delta\psi m$ in fly brains were performed as previously described [12]. Briefly, fly brains were loaded for 40 minutes at room temperature with 40 nM TMRM in loading buffer (10 mM HEPES pH 7.35, 156 mM NaCl, 3 mM KCl, 2 mM $MgSO_4$, 1.25 mM KH_2PO_4, 2 mM $CaCl_2$, and 10 mM glucose), and the dye was present during the experiment. In these experiments, TMRM was used in the redistribution mode for the assessment of $\Delta\psi m$, and therefore, a reduction in the TMRM fluorescence represents mitochondrial depolarization. Confocal images were obtained using a Zeiss LSM 880 confocal microscope equipped with a 40x oil immersion objective. The illumination intensity was kept to a minimum (0.1-0.2% of the laser output) to avoid phototoxicity, and the pinhole was set to yield an optical slice of 2 μm. The fluorescence was quantified by exciting TMRM using the 565-nm laser and measured above 580 nm. Z-stacks of five 300-μm^2 fields were acquired

from each brain, and the mean maximal fluorescence intensity of each group was measured.

Mitochondrial length was quantitated in the enterocytes expressing mitoGFP in the posterior midgut region. Samples were fixed, mounted on Vectashield (Vector Laboratories) and imaged on a Zeiss LSM880 confocal microscope. Mitochondrial length was calculated using the ruler and measurement tools in Photoshop to measure the length of mitoGFP positive mitochondria across their largest dimension.

Analysis of dopaminergic neurons

The brains from 25-day-old flies were dissected and stained with anti-tyrosine hydroxylase antibody (Immunostar, 22941, 1:50) as previously described [67]. The brains were positioned in PBS + 0.1% Triton in a coverslip clamp chamber (ALA Scientific Instruments Inc., NY, USA) using a harp composed of platinum wire and nylon string and imaged by confocal microscopy. The numbers of tyrosine hydroxylase-positive neurons in the PPL1 cluster was determined for each brain hemisphere. The data acquired for the assessment of each genotype were obtained as a single experimental set prior to statistical analysis.

Analysis of food intake

10 adult male flies for each genotype were aged up to 20 days on normal food, changed every 2-3 days. After 20 days, the flies were transferred to food supplemented with 150 µl of 2.5 % bromophenol blue diluted in water, inserted into the food by piercing the surface of the food several times. Bromophenol blue was allowed to diffuse into the food for 24 hours at room temperature. Flies were placed in bromophenol blue-containing food for 16 hours. Following feeding with dye-containing food, the flies were transferred to a pre-weighted empty tube. The tubes with flies were re-weighted, flash frozen in liquid nitrogen and stored at -80^{o}C until processing. Flies were processed by washing 3 times in PBS to remove traces of food on the cuticle (3 times 5 min on a rotating wheel at 4^{o}C). They were then homogenized in 100 µl of PBS using a motor pestle. Homogenates were then centrifuged for 10 min at 16,000 g at 4^{o}C and the supernatant was transferred to a new tube. The absorbance of the supernatant (80 µl) was read at 590 nm using 96-well microtiter plates and an Infinite M200Pro multifunction reader (TECAN, Mannedorf,

Switzerland). The absorbance values were normalised to the weight of the flies. Flies fed with food without bromophenol blue were used as assay blanks.

Metabolic assays

The assessment of DILP2 was performed by ELISA, whereas the levels of TAGs and beta oxidation were assessed through colorimetric assays using 96-well microtiter plates and an Infinite M200Pro multifunction reader (TECAN, Mannedorf, Switzerland).

For the metabolic assays, groups consisting of a maximum of 20 male flies were placed on normal food-containing vials, and the food was changed every 2 days until the desired age was reached, *i.e.*, either 3 or 30 days, and maintained in an 12:12 LD at 25°C. Day 0 was considered the day when the flies emerged from the pupal case. At the defined ageing stage, the flies were transferred into vials containing cotton soaked with water for 2 hours to minimize food contamination from ZT 2 to ZT 4. CO_2-anaesthetized flies were then divided into groups of five flies and flash frozen for subsequent analysis. The TAG assays were essentially performed as previously described [68]. Briefly, for TAG analysis, five adult flies were homogenized in 100 µL of PBS + 0.05% Tween-20 (PBSTw) for 60 seconds on ice and immediately incubated at 70°C for 10 minutes for the inactivation of endogenous enzymatic activity. Forty microlitres of the fly samples and glycerol standards (SIGMA, G7793) were incubated together with either 40 µL of PBST (for free glycerol measurements) or 40 µL of TAG reagent (SIGMA T2449, for TAG measurements) at 37°C for 60 minutes.

After 3 minutes of centrifugation at full speed, 30 µl of each sample (two technical replicates/biological sample) was transferred into a clear-bottom plate together with 100 µL of free glycerol reagent (SIGMA, F6428) at 37°C for 5 minutes.

For insulin ELISA, the flies were maintained and aged as for the TAG assay with the modification that the flies were not starved for 2 hours but rather collected at ZT 2. The ELISA was performed as previously described [37] with the modification that 5 µL of anti-HA-HRP antibody diluted 1:350 in PBS was added to 50 µL of protein samples as described by [69]. Briefly, wells (Thermo Scientific 46867) were coated with 100 µL of anti-FLAG antibody (Sigma, F1804) diluted in 0.2M sodium carbonate/bicarbonate buffer (pH9.4) to a final concentration of 2.5 µg/ml, and incubated overnight at 4°C. Then the plate was washed twice with PBS containing

0.2% Tween 20 (PBTw0.2) for 5mins each, then coated with 350 µL of PBS containing 2% BSA for 16 hours at 4°C. The plate was then washed three times with PBTw0.2. Single fly extract was prepared by placing individual flies in a 1.5 ml Eppendorf tube containing 100 µL of PBS with 1% Triton-X-100. The samples were grounded using a motor pestle on ice and lysed for 30 min at room temperature on a rotary shaker. Samples were then spun at 21000g for 2min at room temperature and surnatant transferred into new tubes. 50 µL of lysate were mixed with 5 µL of anti-HA-HRP (Roche Applied, 12013819001) antibody diluted 1:350 in PBS, vortexed, centrifuged briefly and then added to the pre-coated and pre-blocked ELISA wells overnight at 4°C with gentle agitation. Samples were then removed by aspiration, and wells washed 6 times with PBTw0.2, 100 µL TMB ELISA substrate (Thermo Scientific, 34029) was added to each well and incubated on a rotary sharker for 30 mins in the dark at room temperature. The reaction was stopped by adding 100 µL of 2M sulfuric acid, and the absorbance at 450 nm was immediately measure on the plate reader. Subsequently, the TAG and DILP2 absorbances were divided by the protein concentration of the respective sample, which was measured by the Bradford assay. The results were normalized to the control group by dividing the average values [70].
Similarly, for beta oxidation analysis, 10 flies of the desired age were collected and maintained on ice following the manufacturer's instructions.
For beta oxidation analysis, the flies were maintained and aged as described above with no starvation step and collected at ZT 2. Briefly, 15 flies (for each biological replicate) were anaesthetized, transferred to Eppendorf tubes, weighed and maintained on ice. Approximately 10 mg of tissue was used for each replicate. The flies were subsequently homogenized in 200 µL of provided lysis buffer, and the lysate was clarified by centrifugation at 4°C. The Bradford assay was used for quantification of the protein concentration, and all the samples were normalized to 2 mg/mL. The assay was then performed based on the protocol suggested by the manufacturer (BMR E-141). Incubation at 37°C was performed for 1 hour.
For all Bradford assay a fresh standard curve of BSA (Thermo Scientific, 23210) was prepared for each experiment.

Statistical analyses

The statistical analyses were performed using GraphPad Prism (www.graphpad.com). The data are presented as the mean values, and the error bars indicate the ±SDs. In

violin plots, the solid line represents the median, whereas the dotted lines represent the quartiles. Individual data points in the figures correspond to biological replicates. The number of biological replicates per experimental variable (n) is indicated in either the respective figure or the figure legend. The significance is indicated as follows: * indicates $P < 0.05$, ** indicates $P < 0.01$, *** indicates $P < 0.001$, and **** indicates $P < 0.0001$, NS indicates $P \geq 0.05$.
For all statistical analysis, a normality tests -Saphiro-Wilk test for small ns (<7) and D'Agostino-Pearson (n>7). Based on the normality tests results parametric and non-parametric analyses were chosen accordingly.

Digital image processing

Fluorescence and western blot images were acquired as uncompressed bitmapped digital data (TIFF format) and processed using Adobe Photoshop with established scientific imaging workflows [71]. To visualize the pixel intensity, confocal images acquired with identical settings were processed using a 5-tone heat map (f.64 Academy) in Photoshop.

DATA AVAILABILITY

Source date files, including raw numerical data, descriptive statistics, normality tests and statistical analysis used in the manuscript are available in our GitHub repository at github.com/M1gus/Gut-brain. Microarray data, with detailed descriptions of the experimental protocols, and raw data was deposited in ArrayExpress under accession E-MTAB-6210. The proteomics data was deposited to the ProteomeXchange Consortium with the dataset identifier PXD030979. All other data are available upon reasonable request.

ACKNOWLEDGEMENTS

The proteomics analysis was performed at the Cambridge Centre for Proteomics by Renata Feret, Mike Deery and Yagnesh Umrania. We would like to thank the Vienna *Drosophila* RNAi Center, Bloomington *Drosophila* Stock Center, J. Cordero, A. Telemans, A. Franz and E. Rosato for providing the fly stocks, the Fly Facility, Department of Genetics, University of Cambridge, for maintaining the stocks, and T. Ashby and M. Patel for preparing the fly food. This work was funded by the UK Medical Research Council, intramural project MC_UU_00025/3 (RG94521) to LMM.

The funders had no role in study design, data collection and analysis, decision to publish or preparation of the manuscript.

AUTHOR CONTRIBUTIONS

G.F., I.C., S.H.Y.L. and L.M.M. initiated the project. G.F., S.H.Y.L. and L.M.M. designed the study, coordinated the experiments, and provided conceptual inputs for the paper. G.F., S.H.Y.L. and L.M.M. wrote the manuscript. G.F., I.C., N.S.L., S.L., A.C.C., S.H.Y.L. and L.M.M. performed the experiments and analysed the data. All authors read and approved the final manuscript.

COMPETING INTERESTS

The authors declare no conflicts of interest.

FIGURE LEGENDS

Figure 1. *In silico* identification of Relish as a regulator of transcriptional changes in *pink1*-mutant flies.

(A) Workflow used for the characterization of transcripts and proteins involved in the immune response in *Drosophila pink1*-mutants. Transcripts upregulated by more than two-fold were matched to a list of all genes potentially involved in responses to microbial infection, which are available from the Lemaitre group (lemaitrelab.epfl.ch). After annotation, these genes were matched to the corresponding proteins through global quantitative proteomics analysis. The transcripts were also matched to upstream regulators using the iRegulon algorithm in Cytoscape. (**B**) Relish targets in *pink1*-mutant flies. Transcripts that are potentially involved in the *Drosophila* immune response, as curated by the Lemaitre group, are shown. The iRegulon algorithm predicted that the majority (60%) of the annotated transcripts are regulated by Relish. The detected proteins matched to each of the filtered transcripts are also shown. Transcripts and proteins upregulated by at least two-fold are shown in red colour. ND, not detected; NS, not significant. (**C**) Network visualisation of Relish targets (red) identified by iRegulon. Out of a total of 45 query nodes, 18 were not identified as Relish targets (grey). This figure is related to Supplementary Tables 1, 2, 3 and 4.

Figure 2. Neuronal defects in *pink1*-mutant flies are rescued by genetic and pharmacological inhibition of the immune response.

(**A**) Sleep defects in *pink1*-mutants are suppressed by a *Relish* mutation (asterisks, one-way ANOVA with Tukey's multiple comparison test ($F_{(3, 86)}$=74.88, $P < 0.0001$)). **(B)** Schematic representation of PPL1 anatomical location (upper panel). Representative confocal images of 10 biological replicates showing loss (and rescue) of PPL1 neurons in wild type, *pink*-mutant and *pink1B9; +; RelE20/+* flies (lower panel). **(C)** *Relish* mutation prevents loss of the PPL1 cluster of dopaminergic neurons in *pink1*-mutant flies (means ± SDs; asterisks, Kruskal-Wallis test ($H_{(2,30)}$= 21.49, $P <$ 0.0001) with the Sidak multiple comparison test). **(D, E)** Dietary supplementation with tacrolimus (5 mM) rescues sleep deficits **(D)** (means ± SDs; asterisks, Mann-

Whitney two-tailed test $U_{(40)} = 126$, $P = 0.026$) and the loss of dopaminergic neurons in the PPL1 cluster in *pink1*-mutant flies **(E)** (means ± SDs; asterisks, two-tailed Student's t-test $t_{(23)} = 9.156$, $P < 0.0001$). (**F**) Dietary supplementation with tacrolimus (5mM) does not alter the levels of non-phosphorylated 4E-BP1 in *pink1* mutant nor control flies. Lysates were probed with the indicated antibodies. Levels of non-phosphorylated 4E-BP1 were normalised to actin. Experiments in B and F were performed at least twice with similar results. Genotypes for (A) control: *w; CS/*+, pink1B9: $pink1^{B9}$*; +; +*, pink1B9, RelE20: $pink1^{B9}$*; +;* Rel^{E20}/+, RelE20: *w; +;* Rel^{E20}/+. (B, C) control: *w; CS/*+, pink1B9: $pink1^{B9}$*; +; +*, pink1B9, RelE20: $pink1^{B9}$*; +;* Rel^{E20}/+. (D, E) $pink1^{B9}$*; +; +*. (F) control: *w; CS/*+, pink1B9: $pink1^{B9}$*; +; +*. For descriptive statistics and normality tests refer to the data availability section.

Figure 3. *pink1*-mutant flies show intestinal dysfunction.

(**A**) Representative images of 10 biological replicates showing increased expression of an Attacin-GFP reporter in *pink1*-mutant flies, whereas no detectable expression was observed in age-matched control flies. (**B**) Analysis of gut enterocytes in flies expressing the Attacin-GFP reporter. Representative images of 6 biological replicates are shown. (**C**) The levels of cytosolic Relish in the intestine are decreased in *pink1*-mutant flies. Lysates were probed with the indicated antibodies. Lysates from *Relish*-mutant flies were included to confirm the specificity of the anti-Relish antibody. Four biological replicates of the control and *pink1*-mutant flies were included in the analysis. (**D**) The *Relish* transcript levels are increased in *pink1*-mutants (means ± SEMs; two-tailed Student's *t*-test $t_{(4)}=2.477$, $P = 0.068$), n = 3 biological replicates. (**E**) *pink1*-mutants exhibit a loss of the integrity of their intestinal barrier. The analysis was performed using the Smurf assay. Left: representative images showing a Smurf-positive *pink1*-mutant fly (arrowhead). Right: quantification of Smurf-positive flies. The defects in the intestinal barrier observed in *pink1*-mutant flies are reduced by the *Relish* mutation. The numbers in the bars represent the number of flies tested. Chi-Square two-sided test with Analysis Stack of *P* - values, FDR = 10% (pink1B9 vs RelE20 $\chi^2 = 5.098$, $P = 0.024$, q = 0.0264; pink1B9 vs control $\chi^2=9.274$, P= 0.0023, q= 0.0051; pink1B9 vs pink1B9, RelE20 $\chi^2 = 3.762$, $P = 0.0524$, q = 0.0384; control vs RelE20 $\chi^2 = 0.3241$, $P = 0.5692$, q = 0.2504; control vs pink1B9, RelE20 $\chi^2 =$

1.433, $P = 0.2313$, q = 0.1272). Experiments in A-C were performed at least three times with similar results. Genotypes of (A, B) control: *yw; AttacinA::GFP*, Pink1: *pink1^{B9}; AttacinA::GFP*. (C - E) control: *w; CS/+*, pink1B9: *pink1^{B9}; +; +*, pink1B9, RelE20: *pink1^{B9}; +; Rel^{E20}/+*, RelE20: *w; +; Rel^{E20}/+*. For descriptive statistics and normality tests refer to the data availability section.

Figure 4. Intestinal dysfunction in *pink1*-mutant flies is rescued by a *Relish* mutation.

(**A**) Analysis of the gastrointestinal tract showed a ring of lipids (fat 'doughnut') around the posterior midgut of *pink1*-mutant flies (arrowhead). Purple, phalloidin; Green, BODIPY. An illustration of the imaged region of the gut is shown. (**B** and **C**) Mitochondrial fragmentation in the intestine of *pink1*-mutant flies. Confocal analysis of mitoGFP in the gut enterocytes. Representative confocal images of 5 biological replicates (**B**) and the quantification of mitochondrial length (**C**). The quantification of mitochondrial length is shown as a combined violin and box plot (*P*-value, two-tailed unpaired Mann Whitney test, $U_{(291)} = 4582$, $P < 0.0001$). (**D** and **F**) Caspase activation in the intestine of *pink1*-mutant flies is blocked by a *Relish* mutation. Purple, cell nuclei; Green, Dcp-1. The quantitation of Dcp-1-positive cells in the posterior midgut shows that a *Relish* mutation decreases apoptosis of the enterocytes of *pink1*-mutant flies (means ± SDs; asterisks, Kruskal-Wallis with the multiple comparison test, $H_{(2,33)} = 24.47$, $P < 0.0001$). (**E** and **G**) Increased Escargot expression in the enterocytes of *pink1*-mutant flies (two-tailed Student's t-test, $t_{(23)} = 4.719$, $P < 0.0001$). The gut areas analysed are 425 microns posterior midgut region, just anterior to the Malpighian tubules/hindgut junction. Experiments in A-B and D-E were performed at least three times with similar results. Genotypes in (A-C, D and F) control: *w; CS/+*, pink1B9: *pink1^{B9}; +; +*, pink1B9, RelE20: *pink1^{B9}; +; Rel^{E20}/+*, RelE20: *w; +; Rel^{E20}/+*. (E and G) control: *w; Esg>GFP*; +, Pink1: *pink1^{B9}, Esg>GFP; +*. For descriptive statistics and normality tests refer to the data availability section.

Figure 5. Mutation in a sensor of the innate immune response to DNA rescues the intestinal dysfunction of *pink1*-mutant flies.

(**A**-**B**) Decrease in cytosolic DNA colocalising with mitochondria in *pink1*-mutant flies. Enterocytes expressing mitoGFP were stained with an anti-DNA antibody and Hoechst to visualise the cell nucleus. Representative images of 5 biological replicates (**A**) are shown. Inset areas show examples of cytosolic DNA (red) that does not colocalize with fluorescent mitochondria (green). The colocalisation of DNA with mitochondria (**B)** was assessed using Pearson's correlation coefficients from five regions of interest (ROIs, 10 microns) in each gut (asterisks, one-way ANOVA with Tukey's multiple comparison test, $F_{(2, 30)} = 102.8$, $P < 0.0001$). (**C**) Illustration of the proposed model [11] of the Eya-dependent activation of Relish. Eya associates with IKKβ and Relish in the cytoplasm. The immune response to undigested DNA in flies requires the *eya* gene. (**D**) The eya^2 mutation reduces the expression of the innate immunity transcripts *Attacin-A* (means ± SEMs; asterisks, two-tailed Student's t-test, $t_{(6)} = 4.023$, $P = 0.0069$, n = 4 biological replicates) and *Turandot A* in the intestines of *pink1*-mutant flies (means ± SEMs; asterisks, two-tailed Student's t-test, $t_{(6)} = 2.747$, $P = 0.0334$, n = 4 biological replicates). (**E** and **F**) The eya^2 mutation rescues sleep defects (**E**) and the loss of dopaminergic neurons in the PPL1 cluster (**F**) in *pink1*-mutant flies (means ± SDs; asterisks, one-way Brown-Forsythe ANOVA with multiple comparison test, $F^*(3, 47.83) = 26.48$, $P < 0.0001$(**E**), two-tailed Student's t-test, $t_{(19)} = 8.463$, $P < 0.0001$ (**F**)). Experiment in A was performed at least three times with similar results. Genotypes in (A, B) control: *w; np3084Gal4/+; UASmitoGFP/+*, Pink1: $pink1^{B9}$, *np3084Gal4/+; UASmitoGFP/+*, pink1B9, eya: $pink1^{B9}$; $np3084Gal4/eya^2$; *UASmitoGFP/+*. (C - F) control: *w; CS/+*, pink1B9: $pink1^{B9}$; +; +, pink1B9, eya: $pink1^{B9}$; $eya^2/+$; +, eya: *w;* $eya^2/+$; +. For descriptive statistics and normality tests refer to the data availability section.

Figure 6. *pink1*-mutant flies show increases in metabolic markers of starvation.
(**A**) Insulin-producing neurons (IPCs, blue) are wired between the *Drosophila* nervous system and gut (adapted from [61]). (**B**) Analysis of food intake in 20 days old *pink*-mutant flies (means ± SEMs; two-tailed Student's t-test, $t_{(10)} = 0.8728$, $P = 0.4033$). **(C)** Increased levels of Takeout in *pink1*-mutant flies. The protein levels were

measured by mass spectrometry (means ± SEMs; asterisks, two-tailed Student's t-test, $t_{(8)} = 7.828$, $P < 0.0001$). This figure is related to Supplementary Table 2. (**D**) The upregulation of *Takeout* in aged (30-day-old) *pink1*-mutant flies is partially reversed by a *Relish* mutation (means ± SEMs; asterisks, one-way ANOVA with Tukey's multiple comparison test, $F_{(2,9)} = 46.88$, $P < 0.0001$, n = 4 biological replicates). (**E**) Higher levels of DILP2 are detected in the IPCs of *pink1*-mutant flies, representative images of 7 biological replicates are shown. The intensity levels are visualized using a 5-tone heat map. (**F**) Decreased levels of circulating DILP2 in aged *pink1*-mutant flies (means ± SEMs; asterisks, two-way ANOVA with Tukey's multiple comparison test "Age" $F_{(1,24)} = 6.456$, $P = 0.0179$, "Genotypes" $F_{(1,24)} = 38.23$, $P < 0.0001$, interaction "Age" x "Genotypes" $F_{(1,24)} = 29.67$, $P < 0.0001$). (**G**) Increased levels of circulating triglycerides in both young (3-day-old) (means ± SEMs; asterisks, two-tailed Student's t-test, $t_{(10)} = 2.270$, $P = 0.046$) and old (30-day-old) *pink1*-mutant flies (means ± SEMs; asterisks, two-tailed Student's t-test, $t_{(8)} = 7.060$, $P = 0.0001$). (**H**) *Relish* mutation blocks the age-dependent increase in circulating triglycerides in *pink1*-mutant flies (all genotypes are 30-day-old, means ± SEMs; asterisks, Brown-Forythe ANOVA with multiple comparison test, $F^{*}_{(3,\ 9.722)} = 21.75$, $P = 0.0001$). (**I**) *Relish* mutation does not affect the loss of circulating DILP2 in *pink1*-mutant flies (all genotypes are 30-day-old, means ± SEMs; asterisks, one-way ANOVA with Tukey's multiple comparison test, $F_{(3,24)} = 15.35$, $P < 0.0001$). Experiment in E was performed at least three times with similar results. Genotypes in (B - D, F - I) control: *w; CS/+*, pink1B9: $pink1^{B9}$*; +; +*, pink1B9, RelE20: $pink1^{B9}$*; +;* Rel^{E20}*/+*, RelE20: *w; +;* Rel^{E20}*/+*. (E) control: *w; +; Ilp2/+*, Pink1B9: $pink1^{B9}$*; +; Ilp2/+*. For descriptive statistics and normality tests refer to the data availability section.

Figure 7. The suppression of Relish in the midgut of *pink1*-mutant flies rescues neurodegeneration.

(**A**) The intestinal suppression of Relish reduces the levels of circulating triglycerides in *pink1*-mutants (means ± SEMs; asterisks, two-tailed Student's t-test, $t_{(6)} = 7.510$, $P = 0.0003$). (**B**) Fatty acid oxidation is increased by intestinal suppression of Relish (means ± SDs; asterisks, one-way two-tailed Student's t-test, $t_{(4)} = 4.388$, $P = 0.018$). (**C**) The decrease in cytosolic DNA colocalising with mitochondria in *pink1*-mutants is not blocked by Relish suppression. The colocalisation of DNA with mitochondria in enterocytes was assessed using Pearson's correlation coefficients from five regions

of interest (ROIs, 10 microns) in each gut (asterisks, ANOVA with Tukey's multiple comparisons test, $F_{(2,29)} = 56.31$, $P < 0.0001$). (**D**) Recovery of Δψm following the intestinal suppression of Relish in *pink1*-mutants. Representative confocal images of 8 biological replicates showing whole mounted brains neurons loaded with TMRM. The intensity levels of TMRM are visualized using a 5-tone heat map. The data are shown as the means ± SEMs (n = 5 per genotype; asterisks, Mann Whitney test $U_{(8)} = 0$, $P = 0.0079$). The intestinal suppression of Relish reduces the sleep defects (**E**) (means ± SEMs; asterisks, two-tailed Student's t-test, $t_{(44)} = 2.479$, $P = 0.0171$) and prevents the loss of dopaminergic neurons in the PPL1 cluster of *pink1*-mutants (**F**) (means ± SDs; asterisks, Kruskal-Wallis with the multiple comparison test, $H_{(3,44)} = 35.68$, $P < 0.0001$). (**G**) The RNAi-mediated suppression of Relish using a gut specific driver reduces the levels of Relish mRNA in the intestine (means ± SEMs; asterisks, two-tailed Student's t-test, $t_{(6)} = 3.150$, $P = 0.0198$) but not in the heads of *pink1*-mutants (means ± SEMs; asterisks, Mann-Whitney test, $U_{(34)} = 6$, $P = 0.6857$), n = 4 biological replicates in both tissues. Experiment in D was performed at least three times with similar results. Genotypes in (A, B, D, E and G) Pink1B9; NP3084>: *pink1^{B9}; NP3084Gal4/+*, Pink1B9; NP3084>Rel RNAi: *pink1^{B9}; NP3084Gal4/Rel KK109851.* (C) Control: *w; np3084Gal4/+; UASmitoGFP/+*, PinkB9, NP3084: *pink1^{B9}, np3084Gal4/+; UASmitoGFP/+*, Pink1B9, NP3084> Rel RNAi: *pink1^{B9}; np3084Gal4/RelKK109851; UASmitoGFP/+.* (F) Pink1B9; *pink1^{B9}; +; +;* Pink1B9, NP3084, Rel RNAi: *pink1^{B9}; NP3084Gal4/ Rel KK109851*; Pink1B9, NP1, Rel RNAi: *pink1^{B9}; NP1Gal4/Rel KK109851*; Pink1B9, TH, Rel RNAi: *pink1^{B9}; Rel KK109851/+; THGal4/+*. For descriptive statistics and normality tests refer to the data availability section.

Figure 8. The blockage of intestinal cell death rescues neurodegeneration in *pink1*-mutant flies.

(**A** and **B**) The intestinal expression of Buffy or Pink1 blocks apoptosis in the posterior midgut of *pink1*-mutant flies. (**A**) Representative confocal images of 10 biological replicates showing Dcp-1-positive cells. (**B**) The quantification of Dcp-1-positive cells in the posterior midgut shows that either Buffy or Pink1 reduces the number of Dcp-1-positive enterocytes (means ± SDs; asterisks, one-way ANOVA with the Dunnett's multiple comparison test, $F_{(2,30)} = 25.09$, $P < 0.0001$). (**C**) The intestinal expression of Buffy or Pink1 prevents the loss of dopaminergic neurons in

the PPL1 cluster in *pink1*-mutant flies (means ± SDs; asterisks, one-way ANOVA with the Dunnett's multiple comparison test, $F_{(2,32)} = 20.95$, $P < 0.0001$). (**D**) The RNAi-mediated suppression of pink1 using a gut specific driver reduces the levels of pink1 mRNA in the intestine (two-tailed Student's t-test, $t_{(4)} = 2.737$, $P = 0.0521$) but not in the heads of *pink1*-mutant flies (two-tailed Student's t-test, $t_{(4)} = 0.09992$, $P = 0.9252$), n = 3 biological replicates in both tissues. (**E**) The intestinal suppression of pink1 does not modify the viability of dopaminergic neurons in the PPL1 cluster of aged flies (*P*-value, two-tailed unpaired Mann Whitney test, $U_{(10)} = 56$, $P = 0.4246$). (**F**) The *Bursicon* transcript levels are increased in *pink1*-mutants (asterisks, two-tailed Student's *t*-test $t_{(6)} = 3.898$, $P = 0.0080$, n = 4 biological replicates). Experiment in A was performed at least three times with similar results. Genotypes in (A - C) NP> +: *pink1^{B9}; NP3084Gal4/+;* +, NP > Buffy: *pink1^{B9}; NP3084Gal4/UAS buffy;* +, NP > Pink1; *pink1^{B9}; NP3084Gal4/UAS pink1*. (D, E) NP3084>+: *w; NP3084Gal4/*+, NP3084> Pink1 RNAi: *w; NP3084Gal4/+; pink1 RNAi 31170/*+. (F) pink1B9: *pink1^{B9}; NP3084Gal4/+,* pink1B9; NP3084>Rel RNAi: *pink1^{B9}; NP3084Gal4/ Rel KK10985.* For descriptive statistics and normality tests refer to the data availability section.

REFERENCES

1 Collins, L. V., Hajizadeh, S., Holme, E., Jonsson, I. M. & Tarkowski, A. Endogenously oxidized mitochondrial DNA induces in vivo and in vitro inflammatory responses. *J Leukoc Biol* **75**, 995-1000, doi:10.1189/jlb.0703328 (2004).

2 Celardo, I., Martins, L. M. & Gandhi, S. Unravelling mitochondrial pathways to Parkinson's disease. *British journal of pharmacology* **171**, 1943-1957, doi:10.1111/bph.12433 (2014).

3 Oka, T. *et al.* Mitochondrial DNA that escapes from autophagy causes inflammation and heart failure (vol 485, pg 251, 2012). *Nature* **490**, 292-292, doi:10.1038/nature11515 (2012).

4 Kounatidis, I. *et al.* NF-kappaB Immunity in the Brain Determines Fly Lifespan in Healthy Aging and Age-Related Neurodegeneration. *Cell Rep* **19**, 836-848, doi:10.1016/j.celrep.2017.04.007 (2017).

5 Myllymaki, H., Valanne, S. & Ramet, M. The Drosophila imd signaling pathway. *J Immunol* **192**, 3455-3462, doi:10.4049/jimmunol.1303309 (2014).

6 Molaei, M., Vandehoef, C. & Karpac, J. NF-kappaB Shapes Metabolic Adaptation by Attenuating Foxo-Mediated Lipolysis in Drosophila. *Dev Cell* **49**, 802-810 e806, doi:10.1016/j.devcel.2019.04.009 (2019).

7 Chinchore, Y., Gerber, G. F. & Dolph, P. J. Alternative pathway of cell death in Drosophila mediated by NF-kappaB transcription factor Relish. *Proc Natl Acad Sci U S A* **109**, E605-612, doi:10.1073/pnas.1110666109 (2012).

8 Kuraishi, T., Hori, A. & Kurata, S. Host-microbe interactions in the gut of Drosophila melanogaster. *Front Physiol* **4**, 375, doi:10.3389/fphys.2013.00375 (2013).

9 Sheldon, B. C. & Verhulst, S. Ecological immunology: Costly parasite defences and trade-offs in evolutionary ecology. *Trends Ecol Evol* **11**, 317-321, doi:Doi 10.1016/0169-5347(96)10039-2 (1996).

10 Valtonen, T. M., Kleino, A., Ramet, M. & Rantala, M. J. Starvation Reveals Maintenance Cost of Humoral Immunity. *Evol Biol* **37**, 49-57, doi:10.1007/s11692-009-9078-3 (2010).

11 Liu, X. *et al.* Drosophila EYA regulates the immune response against DNA through an evolutionarily conserved threonine phosphatase motif. *PLoS One* **7**, e42725, doi:10.1371/journal.pone.0042725 (2012).

12 Tufi, R. *et al.* Enhancing nucleotide metabolism protects against mitochondrial dysfunction and neurodegeneration in a PINK1 model of Parkinson's disease. *Nat Cell Biol* **16**, 157-166, doi:10.1038/ncb2901 (2014).

13 Celardo, I. *et al.* Mitofusin-mediated ER stress triggers neurodegeneration in pink1/parkin models of Parkinson's disease. *Cell Death Dis* **7**, e2271, doi:10.1038/cddis.2016.173 (2016).

14 Lemaitre, B. & Hoffmann, J. The host defense of Drosophila melanogaster. *Annu Rev Immunol* **25**, 697-743, doi:10.1146/annurev.immunol.25.022106.141615 (2007).

15 Janky, R. s. *et al.* iRegulon: from a gene list to a gene regulatory network using large motif and track collections. *PLoS Comput Biol* **10**, e1003731 (2014).

16 Julienne, H., Buhl, E., Leslie, D. S. & Hodge, J. J. L. Drosophila PINK1 and parkin loss-of-function mutants display a range of non-motor Parkinson's

disease phenotypes. *Neurobiology of Disease* **104**, 15-23, doi:10.1016/j.nbd.2017.04.014 (2017).
17 Valadas, J. S. *et al.* ER Lipid Defects in Neuropeptidergic Neurons Impair Sleep Patterns in Parkinson's Disease. *Neuron* **98**, 1155-1169 e1156, doi:10.1016/j.neuron.2018.05.022 (2018).
18 Park, J. *et al.* Mitochondrial dysfunction in Drosophila PINK1 mutants is complemented by parkin. *Nature* **441**, 1157-1161 (2006).
19 Hedengren, M. *et al.* Relish, a central factor in the control of humoral but not cellular immunity in Drosophila. *Mol Cell* **4**, 827-837 (1999).
20 Doktor, B., Damulewicz, M., Krzeptowski, W., Bednarczyk, B. & Pyza, E. M. Effects of PINK1 mutation on synapses and behavior in the brain of Drosophila melanogaster. *Acta Neurobiol Exp (Wars)* **78**, 231-241 (2018).
21 Li, Y. X. & Dijkers, P. F. Specific calcineurin isoforms are involved in Drosophila toll immune signaling. *J Immunol* **194**, 168-176, doi:10.4049/jimmunol.1401080 (2015).
22 Tain, L. S. *et al.* Rapamycin activation of 4E-BP prevents parkinsonian dopaminergic neuron loss. *Nat Neurosci* **12**, 1129-1135, doi:nn.2372 [pii] 10.1038/nn.2372 (2009).
23 Han, Z. S. & Ip, Y. T. Interaction and specificity of Rel-related proteins in regulating Drosophila immunity gene expression. *J Biol Chem* **274**, 21355-21361, doi:10.1074/jbc.274.30.21355 (1999).
24 Franz, A., Wood, W. & Martin, P. Fat Body Cells Are Motile and Actively Migrate to Wounds to Drive Repair and Prevent Infection. *Dev Cell* **44**, 460-470 e463, doi:10.1016/j.devcel.2018.01.026 (2018).
25 Karpac, J., Younger, A. & Jasper, H. Dynamic coordination of innate immune signaling and insulin signaling regulates systemic responses to localized DNA damage. *Dev Cell* **20**, 841-854, doi:10.1016/j.devcel.2011.05.011 (2011).
26 Maitra, U., Scaglione, M. N., Chtarbanova, S. & O'Donnell, J. M. Innate immune responses to paraquat exposure in a Drosophila model of Parkinson's disease. *Sci Rep* **9**, 12714, doi:10.1038/s41598-019-48977-6 (2019).
27 Rera, M., Clark, R. I. & Walker, D. W. Intestinal barrier dysfunction links metabolic and inflammatory markers of aging to death in Drosophila. *Proc Natl Acad Sci U S A* **109**, 21528-21533, doi:10.1073/pnas.1215849110 (2012).
28 Suen, D. F., Norris, K. L. & Youle, R. J. Mitochondrial dynamics and apoptosis. *Genes Dev* **22**, 1577-1590, doi:10.1101/gad.1658508 (2008).
29 Naszai, M., Carroll, L. R. & Cordero, J. B. Intestinal stem cell proliferation and epithelial homeostasis in the adult Drosophila midgut. *Insect Biochem Mol Biol* **67**, 9-14, doi:10.1016/j.ibmb.2015.05.016 (2015).
30 Micchelli, C. A. & Perrimon, N. Evidence that stem cells reside in the adult Drosophila midgut epithelium. *Nature* **439**, 475-479, doi:10.1038/nature04371 (2006).
31 Harsh, S., Heryanto, C. & Eleftherianos, I. Intestinal lipid droplets as novel mediators of host-pathogen interaction in Drosophila. *Biol Open*, doi:10.1242/bio.039040 (2019).
32 West, A. P. *et al.* Mitochondrial DNA stress primes the antiviral innate immune response. *Nature* **520**, 553-557, doi:10.1038/nature14156 (2015).
33 Shokri, L. *et al.* A Comprehensive Drosophila melanogaster Transcription Factor Interactome. *Cell Rep* **27**, 955-970 e957, doi:10.1016/j.celrep.2019.03.071 (2019).

34 Sarov-Blat, L., So, W. V., Liu, L. & Rosbash, M. The Drosophila takeout gene is a novel molecular link between circadian rhythms and feeding behavior. *Cell* **101**, 647-656, doi:Doi 10.1016/S0092-8674(00)80876-4 (2000).
35 Ahmad, M., He, L. & Perrimon, N. Regulation of insulin and adipokinetic hormone/glucagon production in flies. *Wiley Interdiscip Rev Dev Biol*, e360, doi:10.1002/wdev.360 (2019).
36 Post, S. *et al.* Drosophila Insulin-Like Peptides DILP2 and DILP5 Differentially Stimulate Cell Signaling and Glycogen Phosphorylase to Regulate Longevity. *Front Endocrinol (Lausanne)* **9**, 245, doi:10.3389/fendo.2018.00245 (2018).
37 Park, S. *et al.* A genetic strategy to measure circulating Drosophila insulin reveals genes regulating insulin production and secretion. *PLoS Genet* **10**, e1004555, doi:10.1371/journal.pgen.1004555 (2014).
38 Heller, S. *et al.* Intestinal inflammation requires FOXO3 and prostaglandin E2-dependent lipogenesis and elevated lipid droplets. *Am J Physiol Gastrointest Liver Physiol* **310**, G844-854, doi:10.1152/ajpgi.00407.2015 (2016).
39 Kim, S. *et al.* Transneuronal Propagation of Pathologic alpha-Synuclein from the Gut to the Brain Models Parkinson's Disease. *Neuron* **103**, 627-641 e627, doi:10.1016/j.neuron.2019.05.035 (2019).
40 Miguel-Aliaga, I., Jasper, H. & Lemaitre, B. Anatomy and Physiology of the Digestive Tract of Drosophila melanogaster. *Genetics* **210**, 357-396, doi:10.1534/genetics.118.300224 (2018).
41 Yin, S., Qin, Q. H. & Zhou, B. Functional studies of Drosophila zinc transporters reveal the mechanism for zinc excretion in Malpighian tubules. *Bmc Biol* **15**, doi:ARTN 12
10.1186/s12915-017-0355-9 (2017).
42 Nehme, N. T. *et al.* A model of bacterial intestinal infections in Drosophila melanogaster. *PLoS Pathog* **3**, 1694-1709, doi:ARTN e173
10.1371/journal.ppat.0030173 (2007).
43 Quinn, L. *et al.* Buffy, a Drosophila Bcl-2 protein, has anti-apoptotic and cell cycle inhibitory functions. *EMBO J* **22**, 3568-3579, doi:10.1093/emboj/cdg355 (2003).
44 Allen, J. F. Control of gene expression by redox potential and the requirement for chloroplast and mitochondrial genomes. *J Theor Biol* **165**, 609-631, doi:10.1006/jtbi.1993.1210 (1993).
45 Sliter, D. A. *et al.* Parkin and PINK1 mitigate STING-induced inflammation. *Nature* **561**, 258-262, doi:10.1038/s41586-018-0448-9 (2018).
46 Meyer, S. N. *et al.* An ancient defense system eliminates unfit cells from developing tissues during cell competition. *Science* **346**, 1258236, doi:10.1126/science.1258236 (2014).
47 Liu, Y. *et al.* Inflammation-Induced, STING-Dependent Autophagy Restricts Zika Virus Infection in the Drosophila Brain. *Cell Host Microbe* **24**, 57-68 e53, doi:10.1016/j.chom.2018.05.022 (2018).
48 Lee, J. J., Andreazza, S. & Whitworth, A. J. The STING pathway does not contribute to behavioural or mitochondrial phenotypes in Drosophila Pink1/parkin or mtDNA mutator models. *Sci Rep* **10**, 2693, doi:10.1038/s41598-020-59647-3 (2020).
49 Petersen, A. J., Katzenberger, R. J. & Wassarman, D. A. The innate immune response transcription factor relish is necessary for neurodegeneration in a

Drosophila model of ataxia-telangiectasia. *Genetics* **194**, 133-142, doi:10.1534/genetics.113.150854 (2013).
50 Lee, H. S., Lobbestael, E., Vermeire, S., Sabino, J. & Cleynen, I. Inflammatory bowel disease and Parkinson's disease: common pathophysiological links. *Gut* **70**, 408-417, doi:10.1136/gutjnl-2020-322429 (2021).
51 Bravo-San Pedro, J. M. & Senovilla, L. Immunostimulatory activity of lifespan-extending agents. *Aging (Albany NY)* **5**, 793-801, doi:10.18632/aging.100619 (2013).
52 Puig, O., Marr, M. T., Ruhf, M. L. & Tjian, R. Control of cell number by Drosophila FOXO: downstream and feedback regulation of the insulin receptor pathway. *Genes Dev* **17**, 2006-2020, doi:10.1101/gad.1098703 (2003).
53 Rynes, J. *et al.* Activating transcription factor 3 regulates immune and metabolic homeostasis. *Mol Cell Biol* **32**, 3949-3962, doi:10.1128/MCB.00429-12 (2012).
54 Song, W. *et al.* Activin signaling mediates muscle-to-adipose communication in a mitochondria dysfunction-associated obesity model. *Proc Natl Acad Sci U S A*, doi:10.1073/pnas.1708037114 (2017).
55 Van Den Berge, N. *et al.* Evidence for bidirectional and trans-synaptic parasympathetic and sympathetic propagation of alpha-synuclein in rats. *Acta Neuropathol* **138**, 535-550, doi:10.1007/s00401-019-02040-w (2019).
56 Scopelliti, A. *et al.* A Neuronal Relay Mediates a Nutrient Responsive Gut/Fat Body Axis Regulating Energy Homeostasis in Adult Drosophila. *Cell Metab* **29**, 269-284 e210, doi:10.1016/j.cmet.2018.09.021 (2019).
57 Melnattur, K., Zhang, B. & Shaw, P. J. Disrupting flight increases sleep and identifies a novel sleep-promoting pathway in Drosophila. *Sci Adv* **6**, eaaz2166, doi:10.1126/sciadv.aaz2166 (2020).
58 Williams, J. A., Sathyanarayanan, S., Hendricks, J. C. & Sehgal, A. Interaction between sleep and the immune response in Drosophila: a role for the NFkappaB relish. *Sleep* **30**, 389-400, doi:10.1093/sleep/30.4.389 (2007).
59 Badinloo, M. *et al.* Overexpression of antimicrobial peptides contributes to aging through cytotoxic effects in Drosophila tissues. *Arch Insect Biochem Physiol* **98**, e21464, doi:10.1002/arch.21464 (2018).
60 Clark, R. I. *et al.* Distinct Shifts in Microbiota Composition during Drosophila Aging Impair Intestinal Function and Drive Mortality. *Cell Rep* **12**, 1656-1667, doi:10.1016/j.celrep.2015.08.004 (2015).
61 Nassel, D. R., Kubrak, O. I., Liu, Y. T., Luo, J. N. & Lushchak, O. V. Factors that regulate insulin producing cells and their output in Drosophila. *Front Physiol* **4**, doi:ARTN 252
10.3389/fphys.2013.00252 (2013).
62 Gatto, L. & Lilley, K. S. MSnbase-an R/Bioconductor package for isobaric tagged mass spectrometry data visualization, processing and quantitation. *Bioinformatics* **28**, 288-289, doi:10.1093/bioinformatics/btr645 (2012).
63 Benjamini, Y. & Hochberg, Y. Controlling the False Discovery Rate: A Practical and Powerful Approach to Multiple Testing. *Journal of the Royal Statistical Society* **57**, 289-300 (1995).
64 Donelson, N. C. *et al.* High-resolution positional tracking for long-term analysis of Drosophila sleep and locomotion using the "tracker" program. *PLoS One* **7**, e37250, doi:10.1371/journal.pone.0037250 (2012).

65 Rera, M. *et al.* Modulation of longevity and tissue homeostasis by the Drosophila PGC-1 homolog. *Cell Metab* **14**, 623-634, doi:10.1016/j.cmet.2011.09.013 (2011).
66 Martins, R. R., McCracken, A. W., Simons, M. J. P., Henriques, C. M. & Rera, M. How to Catch a Smurf? - Ageing and Beyond... In vivo Assessment of Intestinal Permeability in Multiple Model Organisms. *Bio Protoc* **8**, doi:10.21769/BioProtoc.2722 (2018).
67 Whitworth, A. J. *et al.* Increased glutathione S-transferase activity rescues dopaminergic neuron loss in a Drosophila model of Parkinson's disease. *Proc Natl Acad Sci U S A* **102**, 8024-8029 (2005).
68 Tennessen, J. M., Barry, W. E., Cox, J. & Thummel, C. S. Methods for studying metabolism in Drosophila. *Methods* **68**, 105-115, doi:10.1016/j.ymeth.2014.02.034 (2014).
69 Moraru, A. *et al.* Elevated Levels of the Reactive Metabolite Methylglyoxal Recapitulate Progression of Type 2 Diabetes. *Cell Metab* **27**, 926-934 e928, doi:10.1016/j.cmet.2018.02.003 (2018).
70 Zhao, X. & Karpac, J. Muscle Directs Diurnal Energy Homeostasis through a Myokine-Dependent Hormone Module in Drosophila. *Curr Biol* **27**, 1941-1955 e1946, doi:10.1016/j.cub.2017.06.004 (2017).
71 Wexler, E. J. (Lynda.com, Inc., Ventura, 2008).

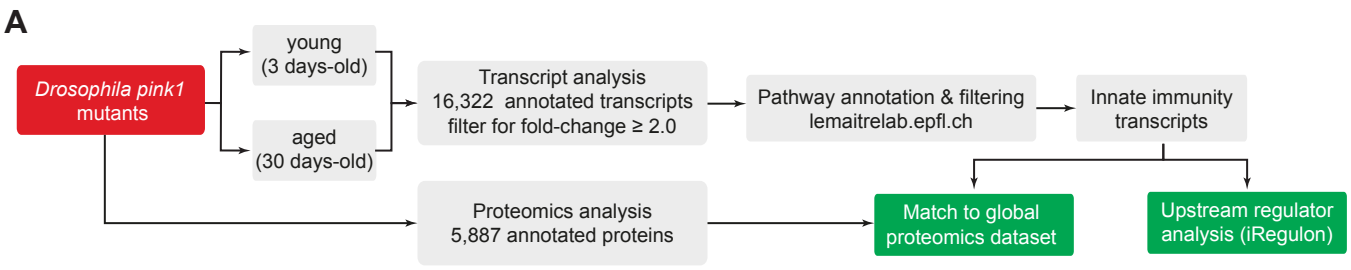

B

	Name	Symbol	mRNA Young	mRNA Aged	Protein	Relish Target?
I	Sensory neuron membrane protein I	Snmp1	■	■	ND	
	PGRP-SC1b	PGRP-SC1b	■		ND	☑
	PGRP-SD	PGRP-SD	■	■		☑
	Scavenger receptor class C, type II	Sr-CII	■	■	ND	
II	Nimrod C1	NimC1	■	■	■	
III	lectin-24A	lectin-24A	■		ND	☑
	lectin-37Da	lectin-37Da	■	■	ND	☑
V	MstProx	MstProx	■		ND	☑
	unpaired 3	upd3		■	ND	☑
	Diedel	Diedel	■	■		
VI	prophenol oxidase A1	proPO-A1	■		ND	
	prophenoloxidase 45	proPO45	■		ND	
VII	CG5550	CG5550	■	■		☑
IX	Lysozyme X	LysX		■		☑
	Attacin-A	AttA	■	■	■	☑
	Drosomycin	Drs		■	■	☑
	Drosomycin-like 3	Drsl3		■	ND	
	Drosomycin-like 4	Drsl4	■	■	■	
	Drosomycin-like 5	Drsl5	■	■	■	
	Metchnikowin	Mtk	■		ND	☑
	Listericin	Listericin		■	ND	☑

	Name	Symbol	mRNA Young	mRNA Aged	Protein	Relish Target?
XI	Turandot A	TotA	■	■	■	
	Turandot C	TotC	■	■	■	
	Turandot M	TotM		■	ND	
XII	CG6639	CG6639		■	ND	
	CG9733	CG9733		■	ND	☑
	Immune induced molecule 1	IM1	■	■	ND	☑
	Immune induced molecule 23	IM23	■	■	■	☑
	CG5791	CG5791	■		ND	☑
	CG14957	CG14957	■	■	ND	
	Immune induced molecule 2	IM2	■	■	ND	☑
	CG4269	CG4269	■	■	ND	☑
	CG9928	CG9928	■		NS	☑
	CG17107	CG17107	■	■		
	CG15065	CG15065	■		ND	☑
	CG9616	CG9616	■	■	ND	☑
	CG9701	CG9701		■	ND	☑
	Urate oxidase	Uro		■	■	
	Gadd45	Gadd45	■		ND	☑
	Arc2	Arc2	■		ND	
	Immune induced molecule 10	IM10	■		ND	☑
	CG9989	CG9989	■	■	ND	☑
	CG13641	CG13641		■	ND	☑
	Cuticular protein 67Fb	Cpr67Fb	■		ND	
	CG10910tTt	CG10910	■		ND	☑

Legend ■ Fold-change ≥ 2 ■ 2 ≥ Fold-change ≥ -2

I - Family of receptors potentially involved in microbial recognition II - Phagocytosis III - Encapsulation V - Signaling VI - Melanization VII - Coagulation IX - Antimicrobial agents XI - Miscellaneous XII - Other genes induced upons sytemic infection (microarray)

C

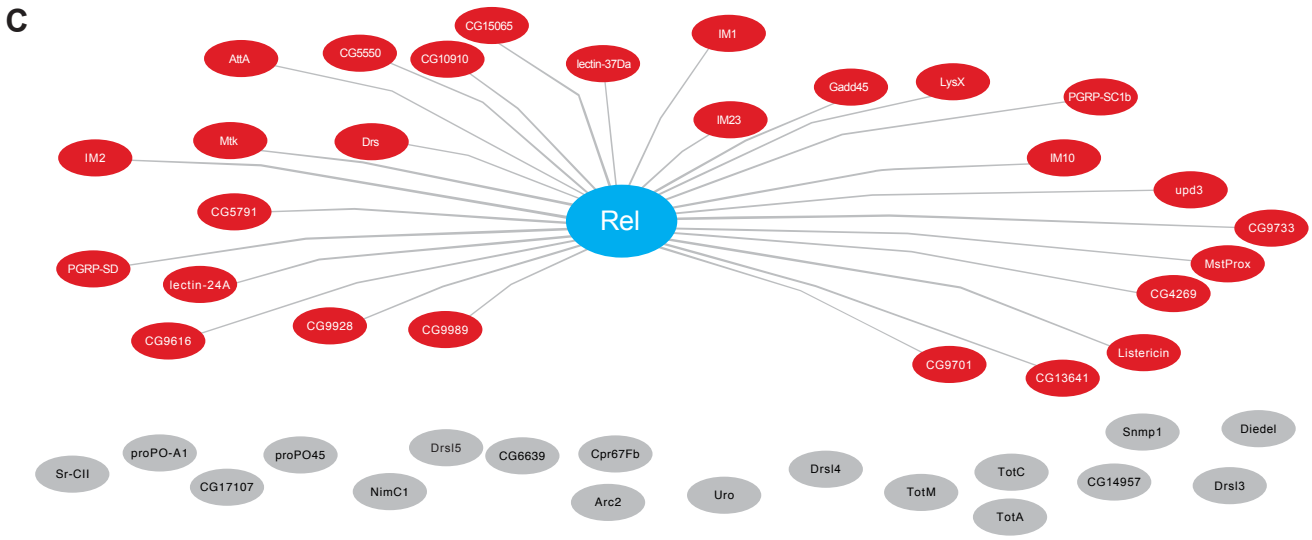

Figure 1

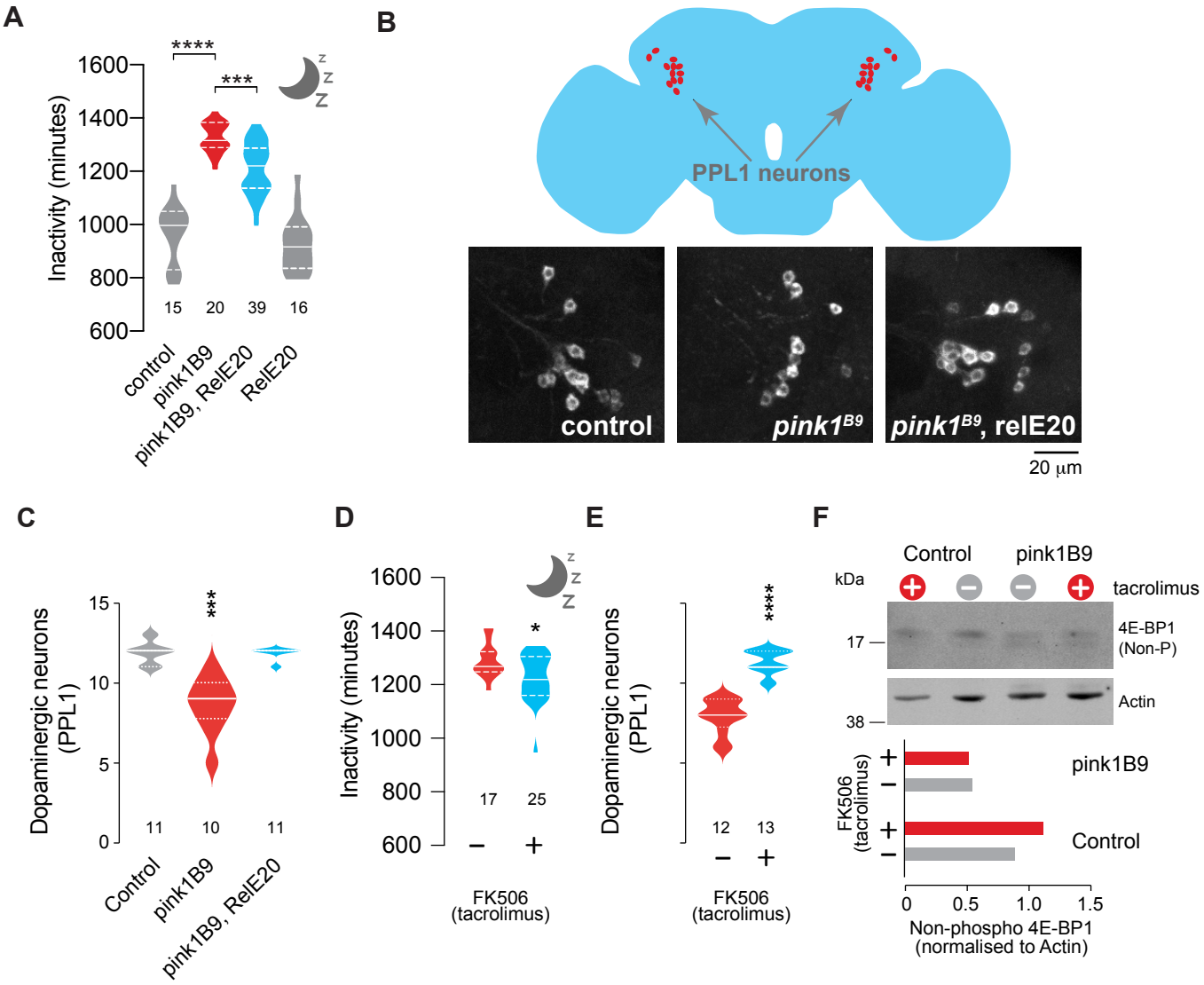
A
B
C
D
E
F
Inactivity (minutes)
1600
1400
1200
1000
800
600
****
***
15
20
39
16
control
pink1B9
pink1B9, RelE20
RelE20
PPL1 neurons
control
pink1B9
pink1B9, relE20
20 µm
Dopaminergic neurons (PPL1)
15
10
5
0
***
11
10
11
Control
pink1B9
pink1B9, RelE20
Inactivity (minutes)
1600
1400
1200
1000
800
600
*
17
25
−
+
FK506 (tacrolimus)
Dopaminergic neurons (PPL1)
****
12
13
−
+
FK506 (tacrolimus)
Control
pink1B9
kDa
tacrolimus
17
4E-BP1 (Non-P)
38
Actin
FK506 (tacrolimus)
+
−
+
−
pink1B9
Control
0
0.5
1.0
1.5
Non-phospho 4E-BP1 (normalised to Actin)

Figure 2

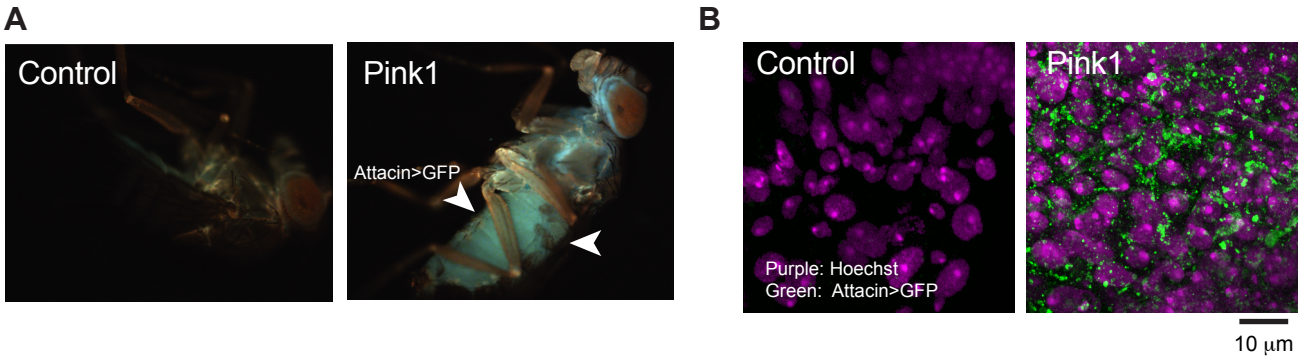
A
Control
Pink1
Attacin>GFP
B
Control
Pink1
Purple: Hoechst
Green: Attacin>GFP
10 μm

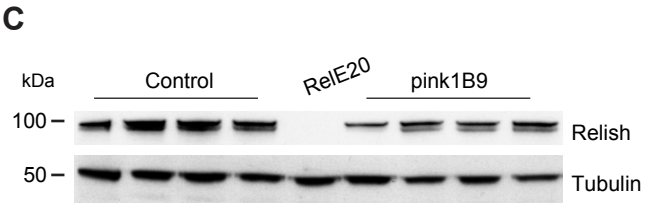
C
kDa
Control
RelE20
pink1B9
100
50
Relish
Tubulin

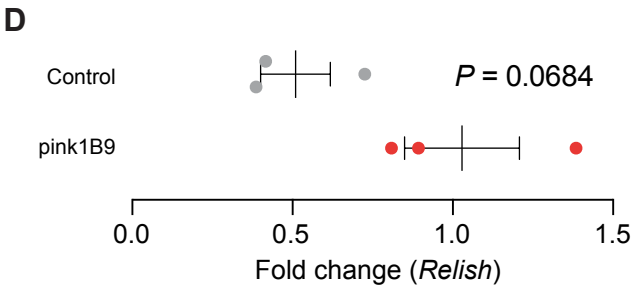
D
Control
pink1B9
P = 0.0684
0.0
0.5
1.0
1.5
Fold change (Relish)


E
Control
Pink1
Smurf

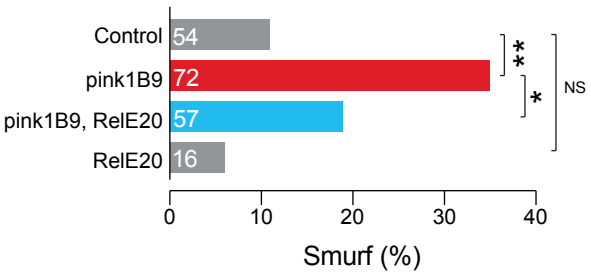
Control
54
pink1B9
72
pink1B9, RelE20
57
RelE20
16
**
*
NS
0
10
20
30
40
Smurf (%)

Figure 3

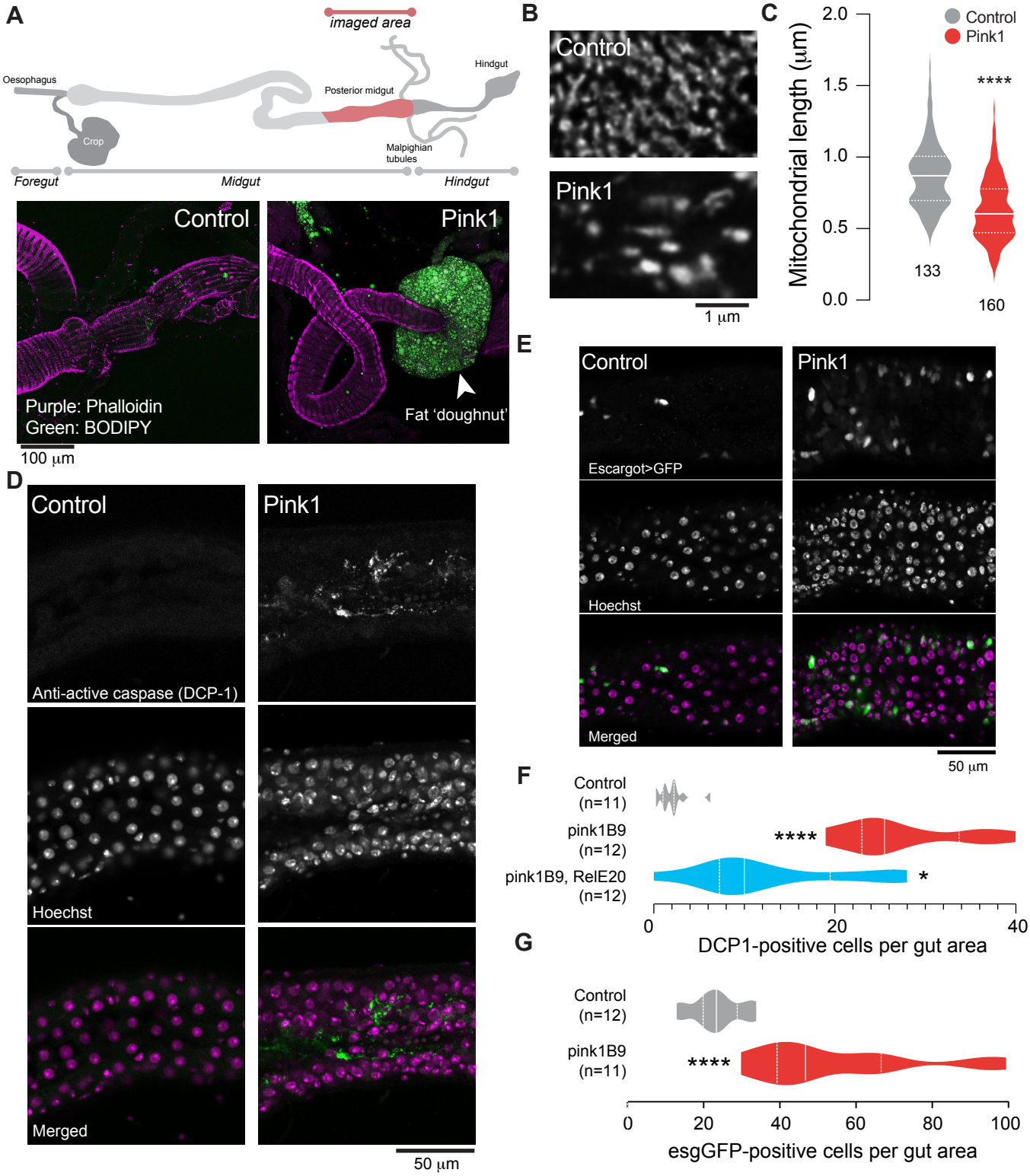
A
imaged area
Oesophagus
Crop
Posterior midgut
Hindgut
Malpighian tubules
Foregut
Midgut
Hindgut
Control
Pink1
Purple: Phalloidin
Green: BODIPY
Fat 'doughnut'
100 μm
B
Control
Pink1
1 μm
C
Mitochondrial length (μm)
2.0
1.5
1.0
0.5
0.0
Control
Pink1
****
133
160
D
Control
Pink1
Anti-active caspase (DCP-1)
Hoechst
Merged
50 μm
E
Control
Pink1
Escargot>GFP
Hoechst
Merged
50 μm
F
Control (n=11)
pink1B9 (n=12)
pink1B9, RelE20 (n=12)
****
*
0
20
40
DCP1-positive cells per gut area
G
Control (n=12)
pink1B9 (n=11)
****
0
20
40
60
80
100
esgGFP-positive cells per gut area

Figure 4

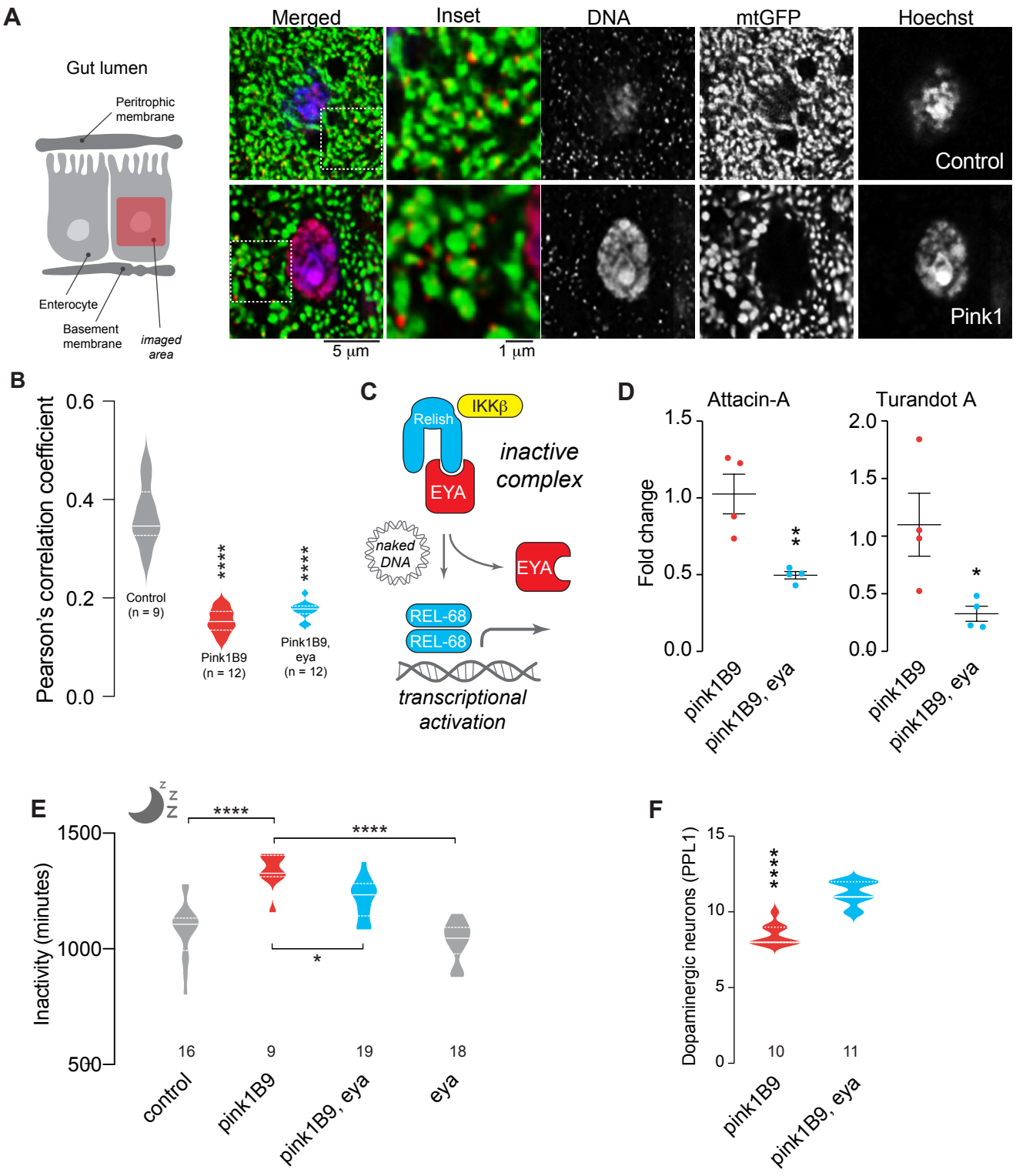
A
Gut lumen
Peritrophic membrane
Enterocyte
Basement membrane
imaged area
Merged
Inset
DNA
mtGFP
Hoechst
Control
Pink1
5 μm
1 μm
B
Pearson's correlation coefficient
0.6
0.4
0.2
0.0
Control (n = 9)
Pink1B9 (n = 12)
Pink1B9, eya (n = 12)
****
****
C
IKKβ
Relish
EYA
inactive complex
naked DNA
EYA
REL-68
REL-68
transcriptional activation
D
Attacin-A
Turandot A
Fold change
1.5
1.0
0.5
0.0
2.0
1.5
1.0
0.5
0.0
**
*
pink1B9
pink1B9, eya
pink1B9
pink1B9, eya
E
Inactivity (minutes)
1500
1000
500
****
****
*
16
9
19
18
control
pink1B9
pink1B9, eya
eya
F
Dopaminergic neurons (PPL1)
15
10
5
0
****
10
11
pink1B9
pink1B9, eya

Figure 5

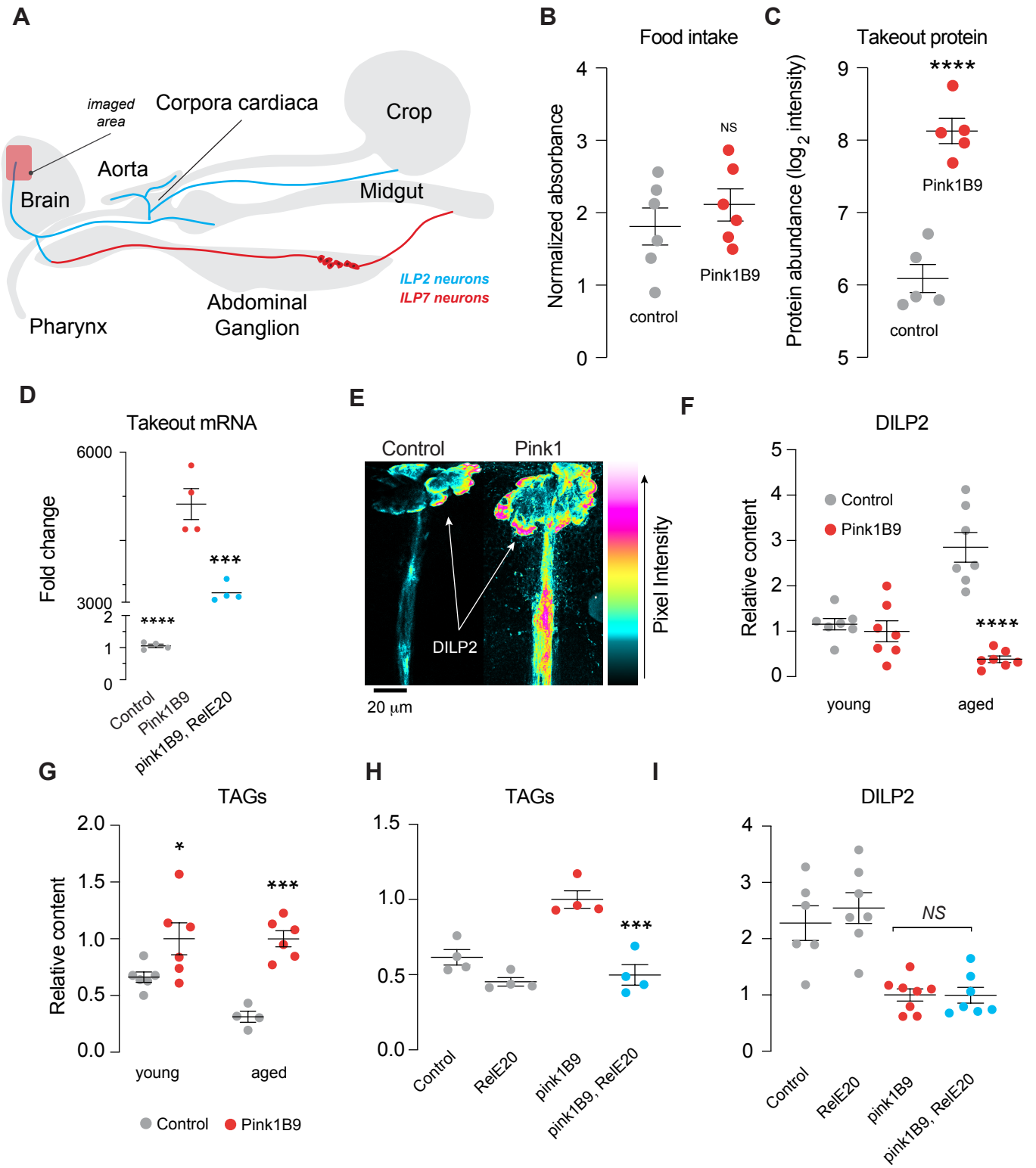
A
imaged area
Corpora cardiaca
Crop
Aorta
Brain
Midgut
ILP2 neurons
ILP7 neurons
Abdominal Ganglion
Pharynx
B
Food intake
Normalized absorbance
NS
control
Pink1B9
C
Takeout protein
Protein abundance (log2 intensity)
****
Pink1B9
control
D
Takeout mRNA
Fold change
****
***
Control
Pink1B9
pink1B9, RelE20
E
Control
Pink1
DILP2
Pixel Intensity
20 µm
F
DILP2
Relative content
Control
Pink1B9
****
young
aged
G
TAGs
Relative content
*
***
young
aged
Control
Pink1B9
H
TAGs
***
Control
RelE20
pink1B9
pink1B9, RelE20
I
DILP2
NS
Control
RelE20
pink1B9
pink1B9, RelE20

Figure 6

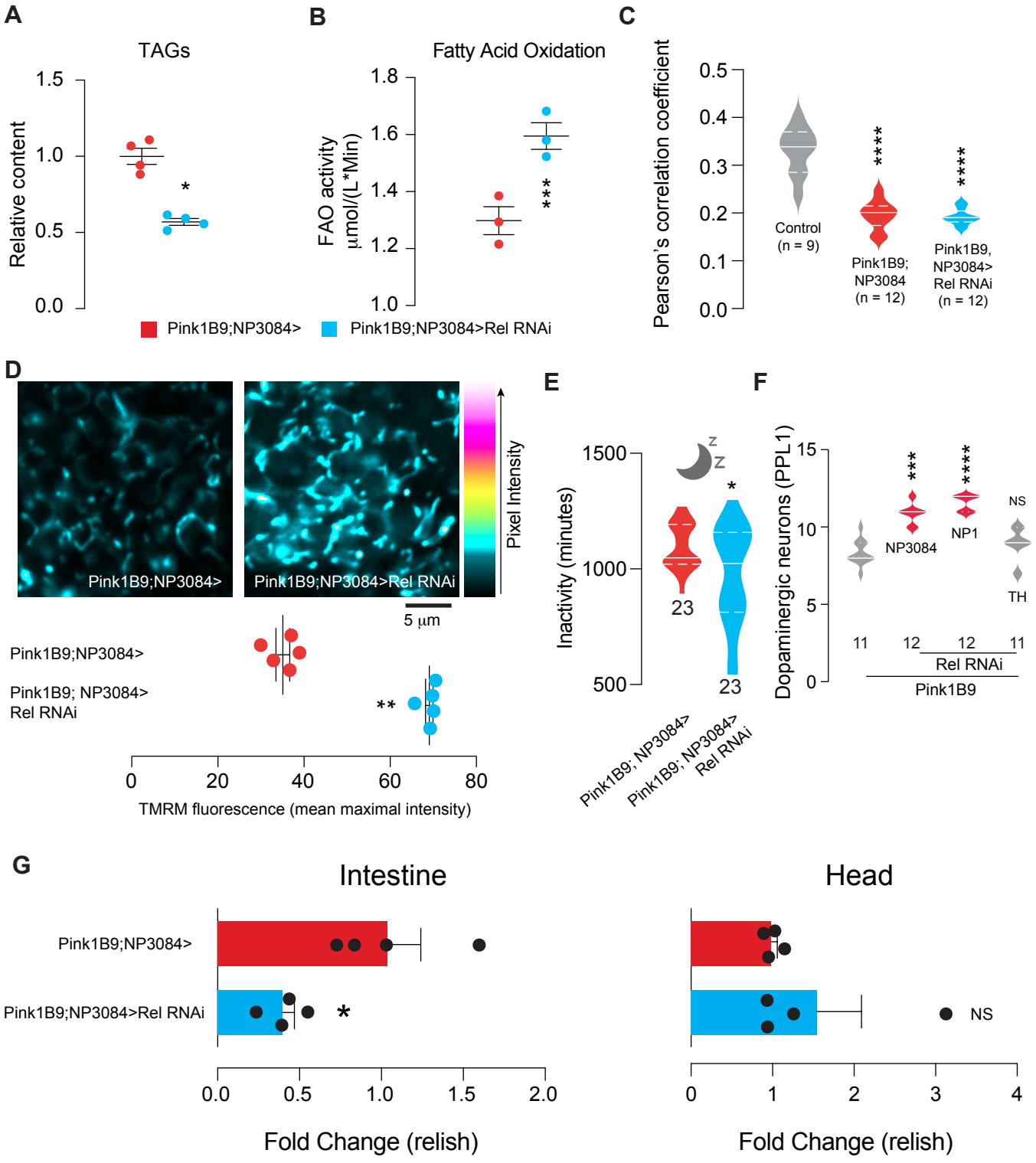
A
TAGs
Relative content
1.5
1.0
0.5
0.0
*
B
Fatty Acid Oxidation
FAO activity µmol/(L*Min)
1.8
1.6
1.4
1.2
1.0
***
Pink1B9;NP3084>
Pink1B9;NP3084>Rel RNAi
C
Pearson's correlation coefficient
0.5
0.4
0.3
0.2
0.1
0.0
Control (n = 9)
****
Pink1B9; NP3084 (n = 12)
****
Pink1B9, NP3084> Rel RNAi (n = 12)
D
Pink1B9;NP3084>
Pink1B9;NP3084>Rel RNAi
Pixel Intensity
5 µm
Pink1B9;NP3084>
Pink1B9; NP3084> Rel RNAi
**
0
20
40
60
80
TMRM fluorescence (mean maximal intensity)
E
Inactivity (minutes)
1500
1000
500
z
z
*
23
23
Pink1B9; NP3084>
Pink1B9; NP3084> Rel RNAi
F
Dopaminergic neurons (PPL1)
15
10
5
0
***
****
NS
NP3084
NP1
TH
11
12
12
11
Rel RNAi
Pink1B9
G
Intestine
Pink1B9;NP3084>
Pink1B9;NP3084>Rel RNAi
*
0.0
0.5
1.0
1.5
2.0
Fold Change (relish)
Head
NS
0
1
2
3
4
Fold Change (relish)

Figure 7

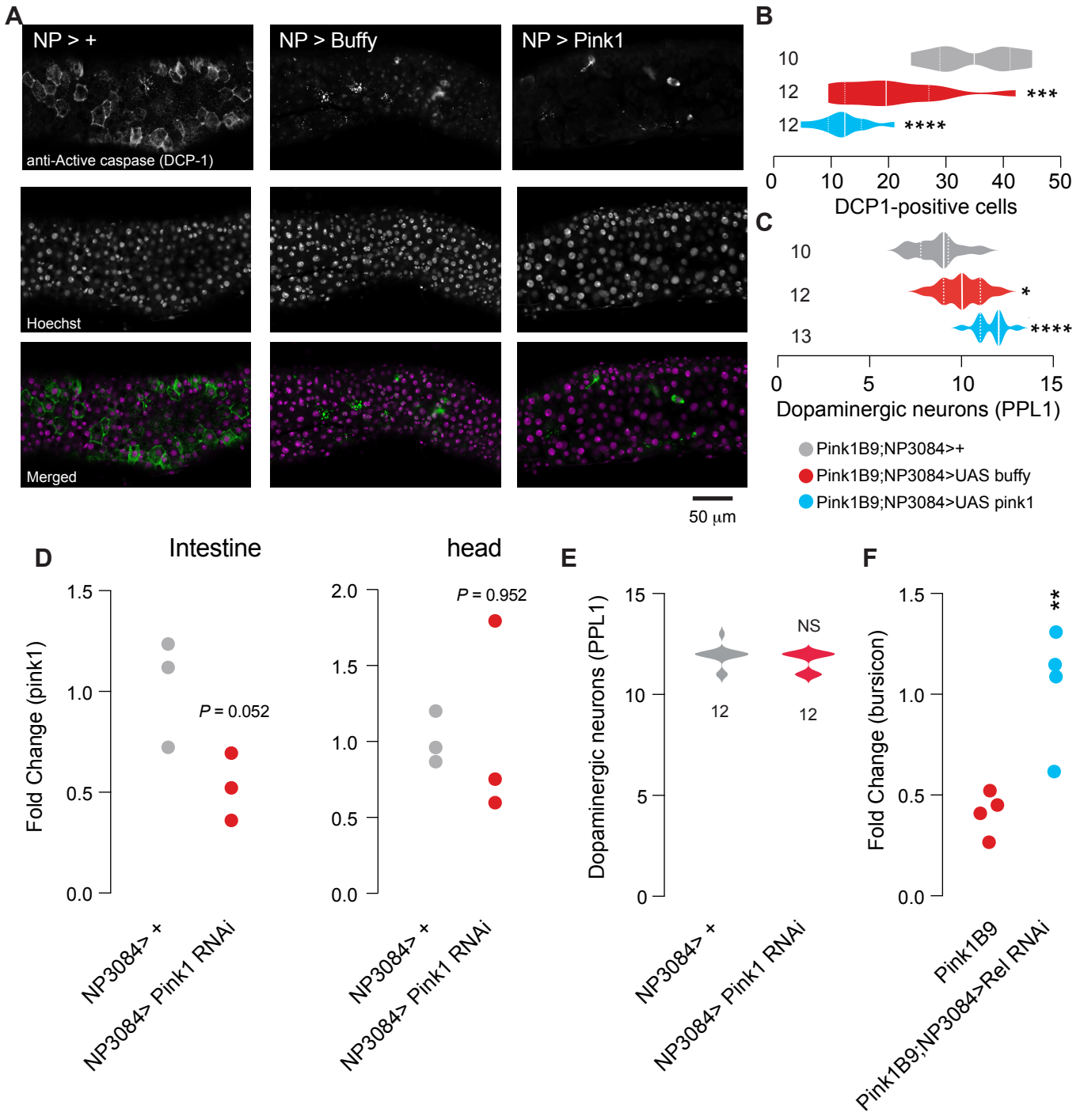
A
NP > +
NP > Buffy
NP > Pink1
anti-Active caspase (DCP-1)
Hoechst
Merged
50 μm
B
10
12
12
***
****
0
10
20
30
40
50
DCP1-positive cells
C
10
12
13
*
****
0
5
10
15
Dopaminergic neurons (PPL1)
Pink1B9;NP3084>+
Pink1B9;NP3084>UAS buffy
Pink1B9;NP3084>UAS pink1
D
Intestine
head
Fold Change (pink1)
P = 0.052
P = 0.952
NP3084> +
NP3084> Pink1 RNAi
E
Dopaminergic neurons (PPL1)
NS
12
12
F
Fold Change (bursicon)
**
Pink1B9
Pink1B9;NP3084>Rel RNAi

Figure 8